STATISTICS, OPTIMIZATION AND INFORMATION COMPUTING
Stat., Optim. Inf. Comput., Vol. **x**, Month 202x, pp 1–27.
Published online in International Academic Press (www.IAPress.org)

Statistical Modelling of Impulse-Excitation Vibration Descriptors for Non-Destructive Characterisation of 3D-Printed PLA: An Exploratory, Orientation-Specific I-kaz^{TM} and M-Z-N Calibration Study

Nadia F. Mohammed [1,*], Ahmed Elloumi [2], M. Z. Nuawi [3], Aref Maalej [2], M. A. F. Ahmad [3], Mohammed T. Jassim [4], Souhail Dhouib [5]

[1]*Department of Mechanical Power Techniques Engineering, College of Technical Engineering, University of Al Maarif, Al Anbar 31001, Iraq*
[2]*Electromechanical Systems Laboratory (LASEM), National Engineering School of Sfax, University of Sfax, Soukra km 4, 3038 Sfax, Tunisia*
[3]*Department of Mechanical Engineering, School of Engineering, Universiti Kebangsaan Malaysia, 43600 UKM Bangi, Selangor, Malaysia*
[4]*Directorate of Military Works*
[5]*Higher Institute of Industrial Management, University of Sfax, Sfax, Tunisia*

Abstract Estimating the mechanical properties of additively manufactured polymer parts currently requires destructive testing, which consumes specimens and scales poorly with the large parameter spaces typical of fused deposition modelling. Vibration-based non-destructive evaluation offers an alternative, but the quantitative link between statistical descriptors of an impulse-excited vibration signal and the mechanical properties of the part has rarely been reported with the model selection and uncertainty quantification that small experimental designs demand. This paper develops and critically evaluates such a link for 3D-printed polylactic acid (PLA). Specimens were fabricated at five infill densities (70, 80, 90, 95 and 100 %) in two raster orientations (L0, L90) and characterised for flexural stress, Young's modulus, apparent density, dynamic shear modulus and Rockwell hardness. Impulse excitation tests (ASTM E1876) were summarised by two statistical descriptors, the Integrated Kurtosis-based Algorithm for Z-notch filter (I-kaz^{TM}) coefficient and the Mesokurtosis Zonal Nonparametric (M-Z-N) coefficient. Ten ordinary least-squares calibrations ($n = 5$ each) were fitted; linear and quadratic specifications were compared by adjusted R^2 and a partial F-test, and the linear form was retained throughout. The strongest relationship was between M-Z-N and hardness for L0 specimens ($R^2 = 0.9901$, $p = 0.0004$), followed by M-Z-N against Young's modulus ($R^2 = 0.9853$, $p = 0.0008$) and against apparent density ($R^2 = 0.9549$, $p = 0.0041$); for L90 specimens I-kaz^{TM} gave $R^2 = 0.9126$ ($p = 0.0113$) with Young's modulus and $R^2 = 0.9088$ ($p = 0.0120$) with density. Two relationships failed to reach the 5 % level: I-kaz^{TM} against flexural stress ($p = 0.0611$) and against hardness ($p = 0.0537$). Inverse calibrations were evaluated by leave-one-out cross-validation, giving $\mathrm{RMSE}_{\mathrm{LOO}}$ of 0.19 GPa for shear modulus and 1.3 HR for hardness in the L0 orientation, against 0.30 GPa and 9.7 HR in L90; in every case the leave-one-out error exceeded the in-sample residual by 44–50 %, which is the direct cost of $n = 5$. Proper 95 % prediction intervals, however, are about three times wider than those cross-validated errors — ±0.57 GPa and ±4.2 HR in L0, and ±0.91 GPa and ±29 HR in L90 — so the L90 hardness relationship cannot serve as a numerical estimator at all. Every descriptor lagged its mechanical counterpart at 90 % infill, which is consistent with the descriptors responding chiefly to the onset of a cellular internal structure rather than to small changes within the near-solid regime although this rests on a single design point. Because M-Z-N was evaluated only on L0 specimens and I-kaz^{TM} only on L90 specimens, method and orientation are confounded and no claim of superiority of either descriptor is made. The relationships are accordingly reported as exploratory, orientation-specific calibrations that support ranking of printing conditions securely and numerical estimation only within the stated intervals. The contribution is a transparent, uncertainty-aware statistical framework linking impulse-excitation signal statistics to five mechanical properties of additively manufactured PLA, together with an explicit statement of the evidence the design can and cannot support.

Keywords 3D-printed PLA, Impulse excitation technique, Vibration signal statistics, I-kaz^{TM}, M-Z-N, Linear regression, Model selection, Leave-one-out cross-validation, Inverse calibration, Non-destructive evaluation

ISSN 2310-5070 (online) ISSN 2311-004X (print)
Copyright © 202x International Academic Press

AMS 2010 subject classifications 62J05, 62P30, 62-08, 94A12

DOI: 10.19139/soic-2310-5070-4699

1. Introduction

Fused deposition modelling (FDM) has moved from prototyping into load-bearing service, and polylactic acid (PLA) is the most widely used feedstock for it because it is biodegradable, inexpensive and easy to process [9, 18]. The mechanical performance of an FDM part, however, is not a property of the feedstock alone. It is determined jointly by the material and by the process parameters that define the internal architecture of the part, principally infill density, raster orientation, layer thickness and deposition temperature [24, 22, 11]. The consequence is anisotropy and part-to-part variability that cannot be read off a material datasheet [2, 30].

Mechanical properties are conventionally established by destructive tests carried out to recognised standards such as ASTM D638 and ASTM D790 [4, 5]. These tests are authoritative, but they destroy the specimen, they are slow, and they require a separate specimen population for every combination of process parameters. For additive manufacturing, where the parameter space is large and the response is anisotropic, the specimen count required for a full characterisation grows quickly [12, 8]. This is the practical motivation for non-destructive evaluation (NDE).

Vibration-based NDE addresses the problem by inferring material behaviour from the dynamic response of an intact specimen; the approach has a long history in the inspection of composites and bonded joints [1]. The impulse excitation technique (IET), standardised in ASTM E1876 [7], excites a freely supported specimen with a light impact and recovers elastic constants from the resonant frequencies [3, 28, 17]. Classical IET is, however, a *modal* method: it uses a small number of spectral peaks and discards the remainder of the transient. Where the specimen is internally porous and anisotropic — as an FDM part with 70 % infill is — the decaying waveform carries information about material continuity and interlayer bonding that a peak-picking analysis does not exploit.

Other non-destructive routes have been applied to additively manufactured polymers, and it is useful to position the present approach against them. Ultrasonic testing recovers elastic constants of FDM PLA from wave velocity, but requires couplant and good surface contact and is sensitive to the internal porosity that sparse infill creates [29]. Experimental modal analysis relates printing parameters to natural frequencies and damping and has recently been combined with response-surface modelling for additively manufactured beams [15]; like classical IET it works from a small number of identified modal parameters. Acoustic emission is a process-monitoring rather than a part-qualification technique. What distinguishes the present route is that it uses the complete decaying transient as a statistical object rather than extracting modal parameters from it, which is why the question of how much usable information the waveform statistics actually carry is the one this paper sets out to quantify.

Statistical signal analysis provides a route to that information. Two descriptors developed at Universiti Kebangsaan Malaysia are relevant here. The Integrated Kurtosis-based Algorithm for Z-notch filter (I-kaz$^{\text{TM}}$) summarises the scatter of a signal about its centroid using the kurtosis and standard deviation of three decomposed components, and returns a single coefficient Z_{∞} [25]. It has been applied to machining monitoring, bearing wear and polymer characterisation [20, 33]. The Mesokurtosis Zonal Nonparametric (M-Z-N) method instead quantifies the zonal dispersion of the discrete signal values about the root-mean-square level of each segment, returning a coefficient Z_{MZN} [26]; it has been used to characterise the elastic and fatigue properties of metals [27, 10]. Both descriptors compress an entire transient into one number, which makes them natural predictors in a regression model.

Three gaps motivate the present work. First, the existing I-kaz$^{\text{TM}}$ and M-Z-N literature is dominated by metals; the few polymer studies are qualitative or cover a narrow property range [33, 23]. Second, where regression relationships between a statistical descriptor and a mechanical property have been reported, they are usually summarised by a single coefficient of determination, without the interval estimates, model-selection evidence or

*Correspondence to: Nadia F. Mohammed (Email: nadia@uoa.edu.iq). Department of Mechanical Power Techniques Engineering, College of Technical Engineering, University of Al Maarif, Al Anbar 31001, Iraq.

residual diagnostics that a calibration with a handful of design points requires. A large R^2 obtained from five points is compatible with a very wide range of underlying associations, and reporting it alone overstates what has been established. Third, the two descriptors are rarely evaluated under matched experimental conditions, so published comparisons between them risk confounding the descriptor with the test configuration.

Motivation. Qualifying an FDM part today means destroying a nominally identical one. For a process whose output depends on at least four interacting parameters, that is both expensive and statistically wasteful: every property reported is a property of a specimen that no longer exists. A descriptor computed from a single impulse response would, if it could be related to mechanical behaviour with a stated uncertainty, allow the part itself to be screened. The barrier is not whether such descriptors respond to internal structure — they plainly do — but whether the relationship is strong enough, and well enough characterised, to be used. That is the question this paper addresses, and it is a statistical question rather than a signal-processing one.

The objective of this study is therefore not simply to demonstrate that vibration statistics correlate with mechanical properties, but to quantify *how strongly, with what uncertainty, and under what conditions* that relationship holds for 3D-printed PLA. The contribution is fivefold: (i) ten ordinary least-squares calibrations linking I-kaz$^{\text{TM}}$ and M-Z-N coefficients to five mechanical properties — flexural stress, Young's modulus, apparent density, dynamic shear modulus and Rockwell hardness — across a 70–100 % infill range in two raster orientations; (ii) a formal linear-versus-quadratic model selection based on adjusted R^2 and a partial F-test rather than on raw R^2; (iii) an uncertainty analysis combining interval estimates for slopes and correlations with leave-one-out cross-validation of the inverse calibrations, which quantifies prediction error rather than fit; and (iv) an explicit classification of the measurement independence of each property, separating relationships in which the descriptor and the property are derived from independent measurements from those in which both derive from the same recorded transient; and (v) proper inverse prediction intervals and residual and influence diagnostics for the four calibrations whose underlying values are tabulated, which show that the honest interval on a property estimated from a descriptor is roughly three times the leave-one-out error. In particular, we identify and report a method–orientation confound in the experimental design that precludes any claim that one descriptor outperforms the other.

Scope of the claims. The design comprises five infill levels per orientation with one specimen each, and no independent validation set. The relationships reported below are therefore presented as *exploratory, orientation-specific calibrations*. They support ranking of printing conditions securely; they support numerical estimation of a property only within the interval widths quantified in Section 3.6, which for one of the four relationships is too wide to be useful. We have preferred to state this at the outset rather than qualify it at the end.

This study belongs to the broader stream of computational and statistical methods applied to engineering decision problems that this journal publishes, which includes heuristic optimisation of robot path planning and of supply-chain networks [13, 14, 21]. Its contribution to that stream is a measurement-calibration counterpart: a regression framework that converts a vibration descriptor into an estimate of a mechanical property with a stated uncertainty.

The remainder of the paper is organised as follows. Section 2 describes the specimens, the destructive and non-destructive measurements, the two statistical descriptors and the regression framework. Section 3 reports the mechanical response, the descriptor behaviour, the fitted calibrations and the model-selection and uncertainty analyses. Section 4 interprets the findings physically and statistically, Section 5 states the limitations, and Section 6 concludes.

2. Materials and methods

2.1. Specimen design and fabrication

Specimens were printed from commercial PLA filament (PolyTerra™ PLA, Polymaker) stored under controlled humidity before use, on an Ender-5 Pro desktop FDM printer. Printing parameters were held constant at a nozzle temperature of 215 °C, a bed temperature of 50 °C and a print speed of 60 mm s^{-1}. A line infill pattern was used throughout.

The experimental design is a two-factor design: infill density at five levels (70, 80, 90, 95 and 100 %) crossed with raster orientation at two levels, 0° and 90° relative to the specimen long axis, denoted L0 and L90 respectively. This gives ten distinct specimen configurations, illustrated in Figure 1.

Two specimen geometries were used, and the distinction matters for the interpretation of the calibrations. Three-point bending specimens followed the ASTM D790 geometry, $125\,\mathrm{mm} \times 12.7\,\mathrm{mm} \times 3.2\,\mathrm{mm}$ (length $\times$ width $\times$ thickness). Impulse excitation was performed on larger rectangular bars, $200\,\mathrm{mm} \times 50\,\mathrm{mm} \times 10\,\mathrm{mm}$, whose dimensions satisfy the slenderness requirement of ASTM E1876. Flexural properties and the vibration descriptors were therefore obtained on *different specimens printed under identical process settings*, not on the same physical part. The calibrations reported in Section 3.3 accordingly relate properties of a printing *condition*, not of an individual specimen, and their residual variance includes between-specimen variability in addition to measurement error.

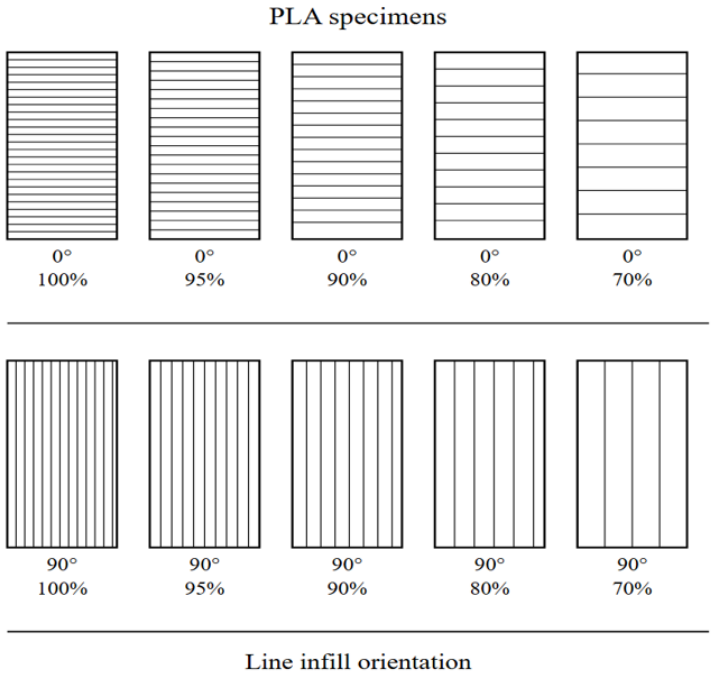


Figure 1. Line-infill architecture of the ten PLA specimen configurations: raster orientations 0° (L0, upper row) and 90° (L90, lower row) at infill densities of 100, 95, 90, 80 and 70 %.

2.2. *Destructive mechanical characterisation*

Three-point bending tests were performed on a universal testing machine following ASTM D790 [5]. Flexural stress was computed from the maximum load as

$$\sigma = \frac{3FL}{2bd^2}, \tag{1}$$

where σ is the flexural stress (MPa), F the applied load (N), L the support span (mm), b the specimen width (mm) and d the specimen thickness (mm).

Young's modulus was obtained from the slope of the initial linear portion of the load–deflection curve,

$$E = \frac{L^3 m}{4bd^3}, \tag{2}$$

where E is Young's modulus (GPa after unit conversion), m the slope of the load–deflection curve in the elastic region (N mm^{-1}), and L, b, d are as in (1).

Specimen density was determined non-destructively by the mass-to-volume method,

$$\rho = \frac{m_s}{V}, \tag{3}$$

where ρ is the measured density (g cm^{-3}), m_s the specimen mass (g) measured on a digital precision balance, and V the volume (cm^3) computed from the measured external dimensions. Note that (3) returns an apparent (bulk) density that includes internal voids, which is the quantity of interest here. Porosity was obtained from the same measurements by comparing the measured mass with the theoretical solid mass $m_{\mathrm{th}} = V\rho_{\mathrm{PLA}}$, taking $\rho_{\mathrm{PLA}} = 1.2\,\mathrm{g\,cm^{-3}}$.

Surface hardness was measured with a Rockwell hardness tester following ASTM D785 [6]. Indentations were taken at several locations on the upper surface of each specimen, away from the perimeter walls, and averaged to give one hardness value per combination of infill density and raster orientation; values are reported in Rockwell units (HR). Two reporting gaps must be stated here, because both were raised in review. First, ASTM D785 defines several Rockwell scales for plastics, and the scale designation used is not recorded in the documentation available for the present analysis; the values are therefore reported in generic Rockwell units and should be compared only within this study, not against values obtained on a named scale elsewhere. Second, the individual indentation readings behind each reported mean were not retained, so no within-specimen standard deviation can be computed and indentation scatter is not propagated into the regression standard errors of Section 3.5. Both consequences are recorded in Section 5.

2.3. *Dynamic elastic constants from resonance*

The dynamic shear modulus G was determined from the torsional resonant frequency of the impulse-excited bar following ASTM E1876 [7],

$$G = \frac{4Lmf_t^2}{bd}\left[\frac{B}{1+A}\right], \tag{4}$$

where f_t is the fundamental torsional resonant frequency (Hz), m the specimen mass (kg), L, b, d the specimen length, width and thickness (m), and A and B are the empirical width-to-thickness correction factors defined in the standard.

2.4. *Impulse excitation and signal acquisition*

Vibration signals were acquired following the procedure of ASTM E1876 [7]. The arrangement is shown in Figure 2. The specimen was supported on thin wires to approximate free–free boundary conditions and minimise external damping, and was excited by a steel ball released from a hook whose height was set once and held constant for all specimens, so that the nominal impulse was the same throughout. Its measured impact-to-impact repeatability was not recorded; see below. Excitation was applied at the specimen mid-span to preferentially excite out-of-plane flexural modes, with the supports located at the nodal points of the fundamental flexural mode, at $0.224L$ from each end.

Two sensors recorded the response simultaneously: a DJB A/23/E accelerometer and a piezofilm sensor mounted near the specimen ends. Both were routed to channels 1 and 2 of a four-channel NI 9234 dynamic signal acquisition module in an NI PXI-1031DC chassis. Acquisition was performed in LabVIEW. Component specifications are summarised in Table 1.

Two aspects of the acquisition chain bear directly on reproducibility and are therefore stated explicitly. The NI 9234 is a 24-bit delta–sigma module with built-in anti-alias filtering whose cut-off tracks the selected sample rate, so the signal chain imposes no filter settings that an operator must choose. Beyond that, the quantities a reader would need in order to reproduce the descriptor values exactly — the sample rate and record length used, whether any further digital filtering was applied before descriptor computation, the number and placement of the signal segments over which (5) and (7) were averaged, and the measured repeatability of the ball-drop impulse

across successive impacts on the same specimen — are not recorded in the documentation available for the present analysis and cannot be recovered from the tabulated results. They are reported here as a documented gap rather than passed over: the descriptor values in Table 2 should be treated as specific to this rig and this acquisition configuration, and a repeatability study with the impulse energy, sensor mounting and segmentation recorded as experimental factors is listed among the priorities for further work (Section 5).

Table 1. Instrumentation and specimen inventory for the impulse excitation tests.

Component	Specification	Quantity
Specimens	PLA, L0 (0°)	5 (one per infill level)
	PLA, L90 (90°)	5 (one per infill level)
Impactor	Steel ball on adjustable-height hook	1
Accelerometer	DJB A/23/E	1
Piezofilm sensor	Surface-mounted polymer film	1
DAQ module	NI 9234, 4-channel	1
DAQ chassis	NI PXI-1031DC	1
Support	Thin suspension wires	2

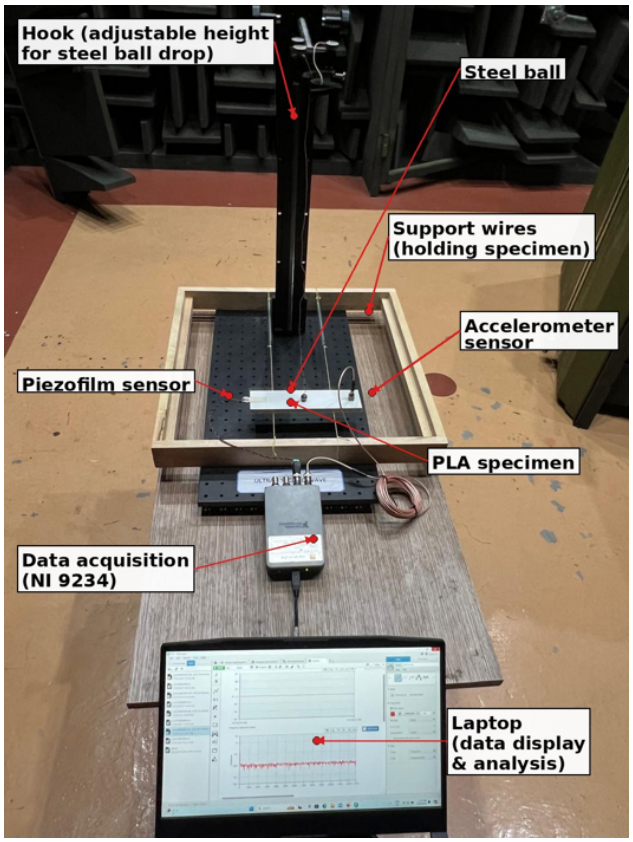


Figure 2. Impulse excitation arrangement: PLA specimen on thin support wires, steel-ball impactor released from an adjustable-height hook, accelerometer and piezofilm sensor, NI 9234 acquisition module.

2.5. Statistical descriptors of the vibration signal

2.5.1. The I-kaz^{TM} coefficient The I-kaz^{TM} method [25] decomposes a time-domain signal into three components and measures the scatter of the resulting three-dimensional data cloud about its centroid. In the I-kaz^{TM} VIBRO variant used here, the three axes are the displacement, velocity and acceleration records derived from the accelerometer channel. The coefficient is

$$Z_{\infty} = \frac{1}{n} \sqrt[4]{K_d S_d^4 + K_v S_v^4 + K_a S_a^4}\,, \tag{5}$$

where n is the number of samples in the analysed record, and K_j and S_j denote respectively the kurtosis (dimensionless) and the standard deviation of component $j \in \{d, v, a\}$, with d = displacement (m), v = velocity (m s^{-1}) and a = acceleration (g units). A larger Z_{∞} indicates a more energetic and more widely dispersed response.

2.5.2. The M-Z-N coefficient The M-Z-N method [26] quantifies the dispersion of the discrete signal values about the root-mean-square (r.m.s.) level, evaluated zonally. The record is divided into M segments of N points; for segment j the r.m.s. level is

$$\mathrm{rms}_j = \sqrt{\frac{1}{N} \sum_{i=1}^{N} x_i^2}, \tag{6}$$

and the coefficient is the mean over segments of the mean squared deviation from that level,

$$Z_{\mathrm{MZN}} = \frac{1}{M} \sum_{j=1}^{M} \left[\frac{1}{N} \sum_{i=1}^{N} \left(x_i - \mathrm{rms}_j\right)^2 \right], \tag{7}$$

where x_i is the ith discrete value in segment j. Both Z_{∞} and Z_{MZN} are reported as dimensionless coefficients.

In the present study M-Z-N was computed for the L0 specimens and I-kaz^{TM} for the L90 specimens. The consequences of this design choice are addressed in Sections 4.6 and 5.

2.6. Measurement independence of the calibrated properties

Not all five properties stand in the same evidential relation to the vibration descriptors, and the distinction must be made explicit before any calibration is interpreted.

Flexural stress σ and Young's modulus E were obtained on a universal testing machine from the load–deflection curve; apparent density ρ was obtained by weighing and measurement; and hardness H was obtained by Rockwell indentation. None of these four quantities is derived from the impulse response. A relationship between one of them and Z_{∞} or Z_{MZN} therefore links two *independent* measurements, and a high coefficient of determination is informative.

The dynamic shear modulus G, by contrast, is computed from the torsional resonant frequency of the same recorded transient from which the descriptors are computed, via (4). The descriptor and the property are then two different functionals of one signal. A strong association between them is partly structural rather than empirical, and the G calibrations must be read as an internal consistency check — a demonstration that a time-domain scatter statistic carries the same stiffness information as a frequency-domain peak — rather than as independent evidence that vibration statistics predict mechanical behaviour. This distinction is carried through Sections 3 and 4 and is not, to our knowledge, made in the existing I-kaz^{TM} and M-Z-N literature.

2.7. Regression framework

For each combination of descriptor and mechanical property, an ordinary least-squares (OLS) model was fitted across the five infill levels,

$$Z_i = \beta_0 + \beta_1 P_i + \varepsilon_i, \qquad i = 1, \ldots, n, \quad n = 5, \tag{8}$$

where Z_i is the statistical descriptor (Z_∞ or Z_{MZN}) for specimen i, P_i is the corresponding mechanical property (flexural stress σ, Young's modulus E, or density ρ), β_0 and β_1 are the intercept and slope, and ε_i is an error term assumed to have zero mean and constant variance.

Two points about (8) require emphasis. First, the response is the *descriptor* and the regressor is the *mechanical property*. This is the natural direction for a calibration experiment, in which the mechanical property is the controlled quantity and the descriptor is measured with error. Estimating a property from a measured descriptor therefore requires the inverse (classical calibration) prediction

$$\hat{P}_0 = \frac{Z_0 - \hat{\beta}_0}{\hat{\beta}_1}, \tag{9}$$

whose uncertainty is not given by the forward residual standard error and is inflated as $\hat{\beta}_1$ approaches zero. Second, because each design point is a single specimen, the error term in (8) confounds measurement error with specimen-to-specimen variability; the two cannot be separated without replication.

2.8. Model selection

The competing quadratic specification

$$Z_i = \beta_0 + \beta_1 P_i + \beta_2 P_i^2 + \varepsilon_i \tag{10}$$

was fitted for each relationship and compared with (8) by three criteria. The adjusted coefficient of determination,

$$R^2_{\mathrm{adj}} = 1 - (1 - R^2)\,\frac{n-1}{n-p-1}, \tag{11}$$

where p is the number of regressors, penalises the loss of residual degrees of freedom; with $n = 5$ the quadratic model retains only two residual degrees of freedom, so the penalty is severe and appropriate. The partial F-test on the additional term,

$$F = \frac{\left(R^2_{\mathrm{quad}} - R^2_{\mathrm{lin}}\right)/1}{\left(1 - R^2_{\mathrm{quad}}\right)/(n-3)} \;\sim\; F_{1,\,n-3} \tag{12}$$

tests whether the curvature is statistically distinguishable from noise. Finally, physical interpretability was considered: within a 70–100 % infill window no saturation plateau or turning point is mechanically expected, since stiffness, apparent density and signal coherence all increase monotonically with the deposited material fraction, so a quadratic term would require a physical mechanism (a critical infill threshold) for which there is no independent evidence.

2.9. Uncertainty quantification

For every retained model we report the sample size n, the fitted equation, the slope and intercept with standard errors, the Pearson correlation r, R^2, R^2_{adj}, the two-sided p-value for $H_0\colon \beta_1 = 0$, and 95 % confidence intervals. The slope interval is $\hat{\beta}_1 \pm t_{0.975,\,n-2}\,\mathrm{SE}(\hat{\beta}_1)$. Because R^2 computed from five points is itself a highly uncertain statistic, an interval estimate for the underlying correlation was obtained by the Fisher variance-stabilising transformation,

$$z = \operatorname{arctanh}(r), \qquad z \pm z_{0.975}\,\frac{1}{\sqrt{n-3}}, \qquad r_{\mathrm{CI}} = \tanh(\cdot), \tag{13}$$

and squared to give an interval for R^2. With $n = 5$ the standard error of z is $1/\sqrt{2} \approx 0.707$, which is large; the resulting intervals are reported in Section 3.9 precisely because they convey the true precision of the calibration.

For the inverse calibrations — those in which a mechanical property is estimated from a measured descriptor — predictive error was assessed by leave-one-out cross-validation. For each design point i the model was refitted on

the remaining four points and used to predict the omitted observation, giving

$$\mathrm{RMSE}_{\mathrm{LOO}} = \sqrt{\frac{1}{n}\sum_{i=1}^{n}\left(y_i - \hat{y}_{-i}\right)^2}, \tag{14}$$

where $\hat{y}_{-i}$ is the prediction for point i from the model fitted without it. At $n = 5$ each refit uses only four points, so $\mathrm{RMSE}_{\mathrm{LOO}}$ is itself a high-variance estimate; it is reported here not as a precise error figure but because the *ratio* $\mathrm{RMSE}_{\mathrm{LOO}}/\mathrm{RMSE}_{\mathrm{fit}}$ exposes how much of the apparent fit is attributable to the fitted point itself.

Cross-validated point errors are not, however, an interval. For each inverse calibration $\hat{y} = a + bx$ the 95 % prediction interval for a single future observation at a measured descriptor value x_0 was therefore computed as

$$\hat{y}_0 \pm t_{0.975,\,n-2}\; s\sqrt{1 + \frac{1}{n} + \frac{(x_0 - \bar{x})^2}{S_{xx}}}, \tag{15}$$

where s is the residual standard error, $\bar{x}$ the mean descriptor value and $S_{xx} = \sum(x_i - \bar{x})^2$. This is the quantity an engineer would need in order to attach a bound to a property estimated from a measured descriptor, and it is reported in Section 3.6. Residual behaviour was examined through the leverage $h_{ii} = 1/n + (x_i - \bar{x})^2/S_{xx}$, the internally studentised residual $r_i = e_i/\left(s\sqrt{1 - h_{ii}}\right)$ and Cook's distance $D_i = \left(r_i^2/2\right)\left(h_{ii}/(1 - h_{ii})\right)$.

We deliberately do *not* describe any model in this paper as validated. No independent specimen set was reserved, and with $n = 5$ a held-out split is not defensible. Leave-one-out cross-validation is an internal diagnostic, not external validation. Formal tests of residual normality and constant variance were not performed: with three residual degrees of freedom they have essentially no power, and reporting a non-significant Shapiro–Wilk statistic from five residuals would convey false reassurance. Bayesian calibration with weakly informative priors, or bootstrap resampling, would in principle propagate small-sample uncertainty more honestly than the classical intervals used here; both are identified in Section 5 as the natural methodological extension once replicated data exist, since neither can manufacture information that five design points do not contain.

2.10. Software

Signal acquisition and time-domain processing were performed in LabVIEW and NI FlexLogger (National Instruments). Descriptor computation used the I-kaz™ and M-Z-N routines developed at Universiti Kebangsaan Malaysia and described in [25, 26]. Every regression, model-selection, interval and diagnostic statistic reported in this paper — the fitted coefficients and their standard errors, the adjusted R^2 and partial F comparisons (11)–(12), the Fisher intervals (13), the leave-one-out errors (14), and the prediction intervals and influence diagnostics (15) — was recomputed independently from the tabulated measurements in Python 3.13 using NumPy 2.5 and SciPy 1.18, and reproduced the values obtained in the original analysis. The measured values underlying the four calibrations analysed in Section 3.6 are tabulated in Tables 2 and 4, so that those fits, their intervals and their diagnostics can be reproduced directly from the paper.

3. Results

3.1. Mechanical response to infill density and raster orientation

All three measured properties increased monotonically with infill density over the 70–100 % range, in both orientations (Figures 4 and 5). Flexural stress rose from 11.347 MPa at 70 % infill in the L0 orientation to 58.458 MPa at 100 % infill in the L90 orientation. Young's modulus increased from 0.471 GPa (L0, 70 %) to 3.263 GPa (L0, 100 %), a factor of 6.9, and from 2.256 GPa to 3.344 GPa, a factor of 1.5, over the same range in the L90 orientation. Apparent density increased from 0.892 4 g cm^{-3} to 1.237 7 g cm^{-3} for L0 and from 0.889 2 g cm^{-3} to 1.238 6 g cm^{-3} for L90; the 100 % values agree with the nominal bulk density of PLA ($\approx 1.24\,\mathrm{g\,cm^{-3}}$) to within 0.3 %, indicating that fully dense printing produced few residual voids.

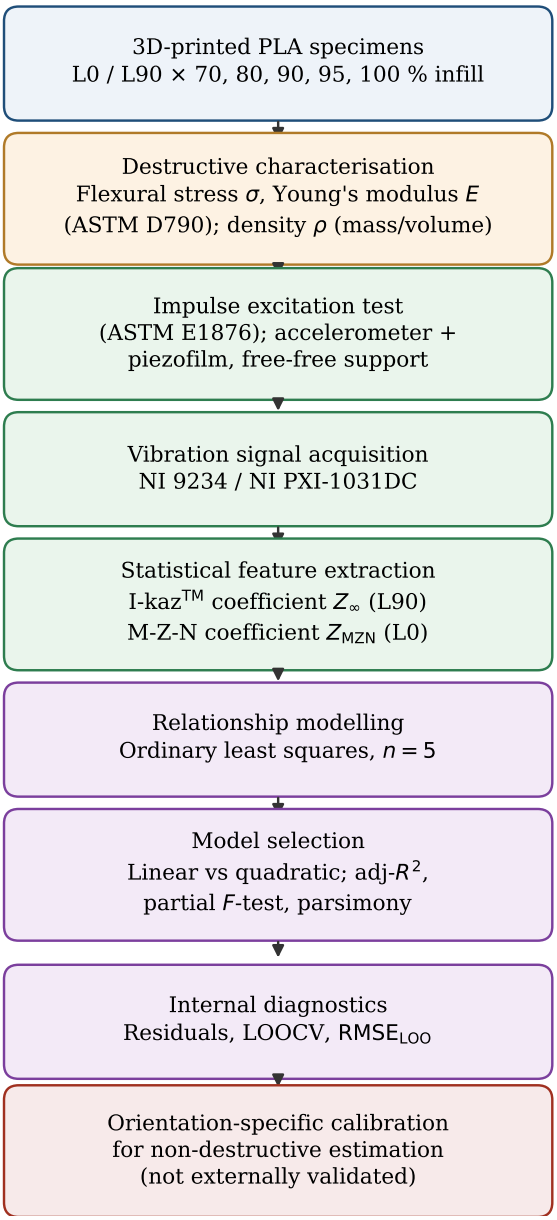


Figure 3. Analysis workflow, from specimen fabrication through destructive and non-destructive measurement to statistical feature extraction, relationship modelling, model selection and orientation-specific calibration.

The two orientations respond very differently. Density is essentially orientation-independent: L0 and L90 values agree to within approximately 1 % at every infill level, which is expected because raster orientation changes the direction of deposition but not the volume of deposited material. Stiffness and strength, by contrast, are strongly orientation-dependent, and the gap widens as infill decreases. At 100 % infill the two orientations give almost the same modulus (3.263 versus 3.344 GPa, a difference of 2.5 %), whereas at 70 % infill the L90 modulus is roughly 4.8 times the L0 value (2.256 versus 0.471 GPa). Because the material content is the same in both orientations, this

divergence is attributable to filament alignment relative to the bending load rather than to differences in the amount of material present.

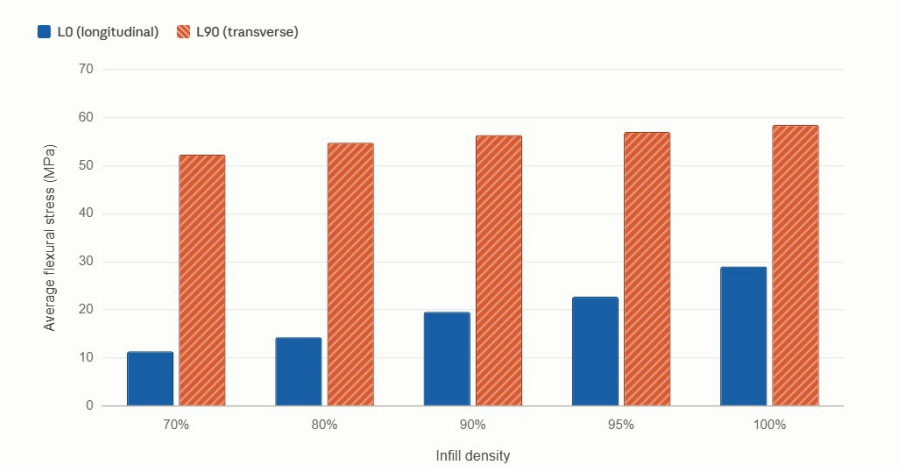


Figure 4. Average flexural stress (MPa) as a function of infill density for the L0 (0°) and L90 (90°) raster orientations. One specimen per configuration; no error bars are shown because the design contains no replicates.

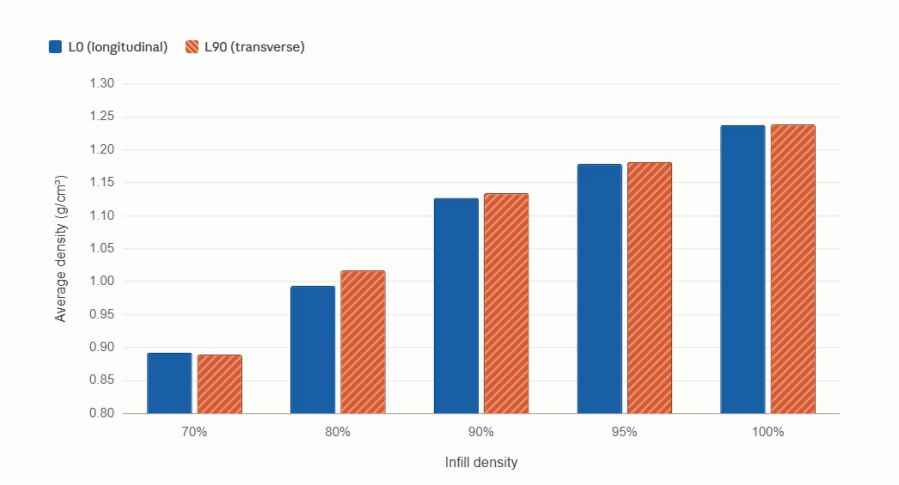


Figure 5. Average apparent specimen density (g cm^{-3}) as a function of infill density and raster orientation.

3.2. Vibration signals and descriptor behaviour

Figure 6 shows a representative pair of time histories and their Fourier spectra. Both channels record a high-amplitude transient followed by an exponential decay characteristic of a lightly damped free response. The first flexural resonance is identified at 407.9 Hz in both the accelerometer and the piezofilm spectrum, with further peaks above 2 kHz corresponding to higher-order modes. Agreement between two independent transducers at the fundamental frequency confirms that the acquisition chain resolves the specimen response reliably, which is a precondition for the descriptor analysis that follows.

Both descriptors increase monotonically with infill density (Figure 7). The M-Z-N coefficient of the L0 specimens rises from 0.0832 at 70 % to 0.1746 at 100 %, an increase of 110 %; the I-kaz^{TM} coefficient of the L90

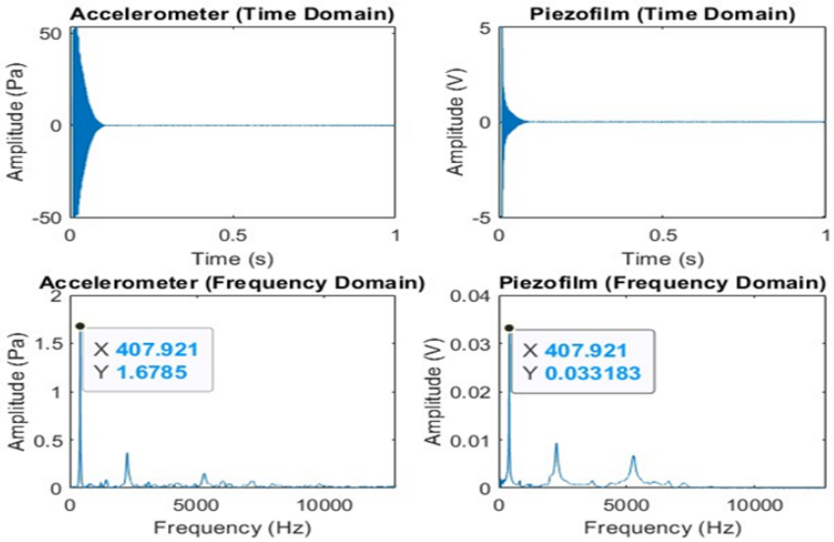


Figure 6. Representative impulse response of a PLA specimen. Top: time-domain records from the accelerometer (left) and piezofilm sensor (right). Bottom: corresponding Fourier spectra, with the fundamental flexural resonance at 407.9 Hz in both channels.

specimens rises from 9.90×10^{-6} to 20.00×10^{-6}, an increase of 102 %. In both cases the largest single increment occurs between 80 and 90 % infill (+65 % for M-Z-N, +69 % for I-kaz$^{\text{TM}}$), consistent with a transition from a visibly porous internal structure to a nearly continuous one. The two descriptors therefore exhibit comparable sensitivity to material continuity despite being computed on specimens of different raster orientation. Descriptor values are listed in Table 2.

Table 2. Statistical descriptor values as a function of infill density. M-Z-N was computed on L0 specimens and I-kaz$^{\text{TM}}$ on L90 specimens; both coefficients are dimensionless.

Infill density (%)	Z_{MZN} (L0)	Increment (%)	$Z_\infty \times 10^6$ (L90)	Increment (%)
70	0.0832	—	9.90	—
80	0.0955	+14.8	10.70	+8.1
90	0.1577	+65.1	18.10	+69.2
95	0.1606	+1.8	18.20	+0.6
100	0.1746	+8.7	20.00	+9.9
Total change	+110 %		+102 %	

3.3. Calibration relationships

Six OLS models of the form (8) were fitted. The complete set of estimates is consolidated in Table 3, which is the central statistical result of this paper.

3.3.1. M-Z-N calibrations for L0 specimens For the L0 specimens, the M-Z-N coefficient is strongly and positively associated with all three properties (Figure 8). The strongest relationship is with Young's modulus,

$$\hat{Z}_{\text{MZN}} = 0.07284 + 0.03262\,E, \qquad n = 5,\ R^2 = 0.9853,\ p = 0.0008, \tag{16}$$

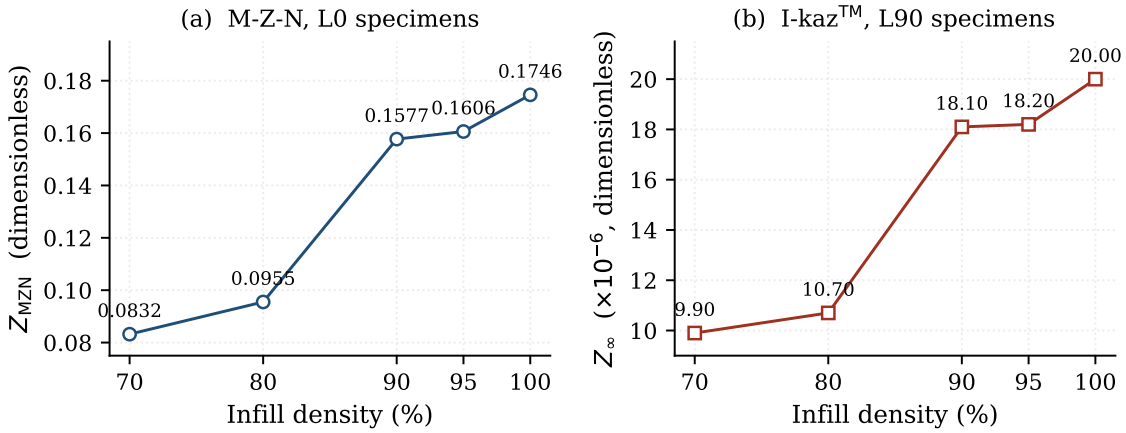


Figure 7. Statistical descriptors as a function of infill density: (a) M-Z-N coefficient for L0 specimens; (b) I-kaz™ coefficient for L90 specimens. Both increase monotonically, with the largest increment between 80 and 90 % infill.

Table 3. Consolidated linear calibration statistics ($n = 5$ for every model; $\mathrm{df} = 3$). Slopes are reported per unit of the mechanical property; p is the two-sided test of $H_0 : \beta_1 = 0$. Confidence intervals for R^2 were obtained via the Fisher transformation (13) and are wide because $n = 5$.

Property → descriptor	Orient.	Slope $\hat{\beta}_1$	SE	95% CI for β_1	Intercept $\hat{\beta}_0$	r	R^2	R^2_{adj}	p
Flexural stress → Z_{MZN}	L0	5.66×10^{-3}	1.25×10^{-3}	$[1.68, 9.64] \times 10^{-3}$	2.413×10^{-2}	0.9341	0.8725	0.8300	0.0201
Young's modulus → Z_{MZN}	L0	3.262×10^{-2}	2.09×10^{-3}	$[2.60, 3.93] \times 10^{-2}$	7.284×10^{-2}	0.9926	**0.9853**	0.9804	0.0008
Density → Z_{MZN}	L0	2.8986×10^{-1}	3.64×10^{-2}	$[1.74, 4.06] \times 10^{-1}$	-1.8046×10^{-1}	0.9772	**0.9549**	0.9399	0.0041
Flexural stress → Z_∞	L90	1.832×10^{-6}	6.26×10^{-7}	$[-0.16, 3.82] \times 10^{-6}$	-8.616×10^{-5}	0.8607	0.7409	0.6545	**0.0611**
Young's modulus → Z_∞	L90	1.0662×10^{-5}	1.90×10^{-6}	$[0.46, 1.67] \times 10^{-5}$	-1.5038×10^{-5}	0.9553	**0.9126**	0.8835	0.0113
Density → Z_∞	L90	3.211×10^{-5}	5.87×10^{-6}	$[1.34, 5.08] \times 10^{-5}$	-1.9694×10^{-5}	0.9533	**0.9088**	0.8784	0.0120

Units: flexural stress in MPa; Young's modulus and shear modulus in GPa; density in g cm^{-3}; hardness in Rockwell units (HR). Descriptors are dimensionless, so slopes carry units of (dimensionless)/(property unit). †Shear modulus is derived from the torsional resonance of the same transient that yields the descriptor; these two rows are internal consistency checks, not independent calibrations (Section 2.6).

with E in GPa. The relationship with apparent density is

$$\hat{Z}_{\mathrm{MZN}} = -0.18046 + 0.28986\,\rho, \qquad n = 5,\ R^2 = 0.9549,\ p = 0.0041, \tag{17}$$

with ρ in g cm^{-3}, and with flexural stress

$$\hat{Z}_{\mathrm{MZN}} = 0.02413 + 0.00566\,\sigma, \qquad n = 5,\ R^2 = 0.8725,\ p = 0.0201, \tag{18}$$

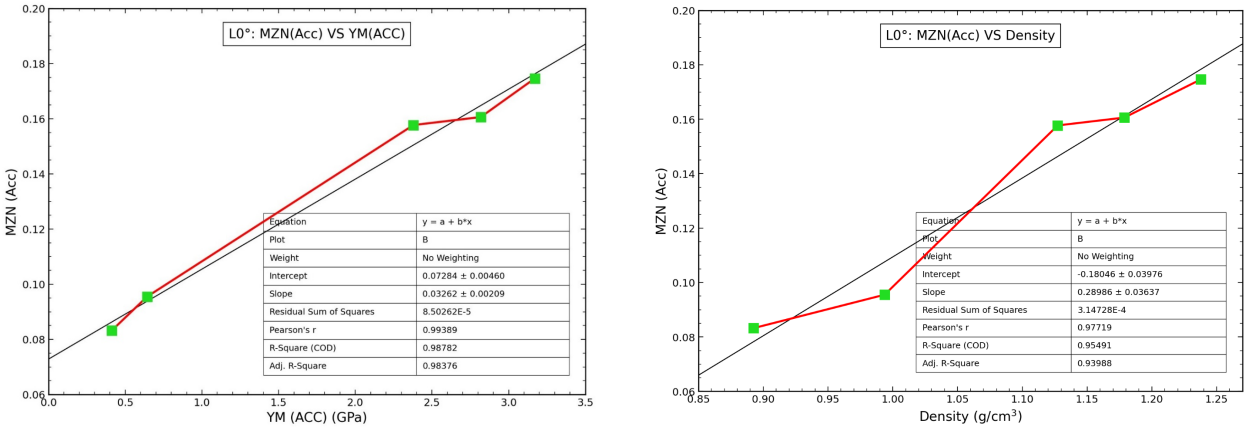
with σ in MPa. All three slopes are significantly different from zero at the 5 % level, and the ordering ($E > \rho > \sigma$) is consistent across R^2, p and the relative width of the slope interval.

3.3.2. I-kaz™ calibrations for L90 specimens For the L90 specimens, the I-kaz™ coefficient is significantly associated with Young's modulus,

$$\hat{Z}_\infty = -1.5038 \times 10^{-5} + 1.0662 \times 10^{-5}\,E, \qquad n = 5,\ R^2 = 0.9126,\ p = 0.0113, \tag{19}$$

and with apparent density,

$$\hat{Z}_\infty = -1.9694 \times 10^{-5} + 3.211 \times 10^{-5}\,\rho, \qquad n = 5,\ R^2 = 0.9088,\ p = 0.0120. \tag{20}$$



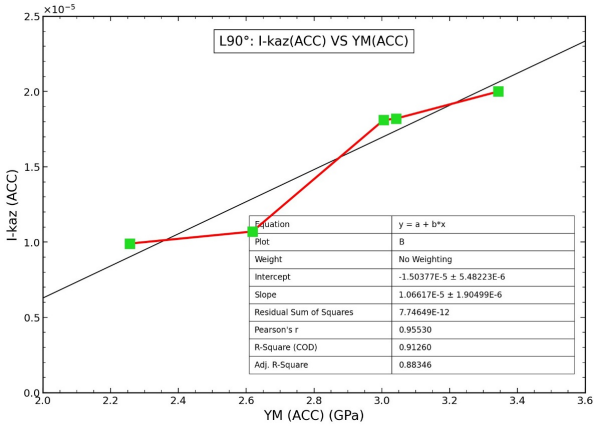
(a) Young's modulus (b) Apparent density

Figure 8. M-Z-N calibration relationships for L0 specimens. Observed values (markers), fitted least-squares line and regression statistics.

The relationship with flexural stress is weaker and, critically, *not* significant at the 5 % level:

$$\hat{Z}_\infty = -8.616 \times 10^{-5} + 1.832 \times 10^{-6}\,\sigma, \qquad n = 5,\ R^2 = 0.7409,\ p = 0.0611. \tag{21}$$

The 95 % confidence interval for the slope in (21), $[-0.16,\ 3.82] \times 10^{-6}$, includes zero. **This relationship does not reach the conventional 5 % significance level and is not a calibration.** It is reported here only so that the full set of ten fitted relationships is visible, and it is labelled as non-significant wherever it appears. No inference in this paper rests on it, and it should not be used to estimate flexural stress. This relationship should therefore be described as suggestive rather than established, and it is the one relationship in Table 3 that does not support a calibration claim.



(a) Young's modulus

Figure 9. I-kaz^{TM} calibration of Young's modulus for L90 specimens: observed values (markers), fitted least-squares line and regression statistics.

3.4. *Shear modulus and hardness*

Two further properties were characterised across the same design. Both decrease monotonically with infill density in both orientations (Figure 10, Table 4).

Table 4. Dynamic shear modulus G and Rockwell hardness H versus infill density, with the percentage retained relative to 100 % infill and the ratio between orientations.

Infill (%)	G_{L0} (GPa)	G_{L90} (GPa)	G_{L90}/G_{L0}	H_{L0} (HR)	H_{L90} (HR)	H_{L90}/H_{L0}	ΔG_{L0} (%)	ΔH_{L0} (%)
100	2.010	1.973	0.982	75.12	70.80	0.942	0.0	0.0
95	1.839	1.785	0.971	73.32	62.16	0.848	−8.5	−2.4
90	1.474	1.227	0.832	69.76	46.52	0.667	−26.7	−7.1
80	1.082	0.899	0.831	56.10	40.05	0.714	−46.2	−25.3
70	0.893	0.723	0.810	52.46	36.30	0.692	−55.6	−30.2

Δ denotes change relative to 100 % infill.

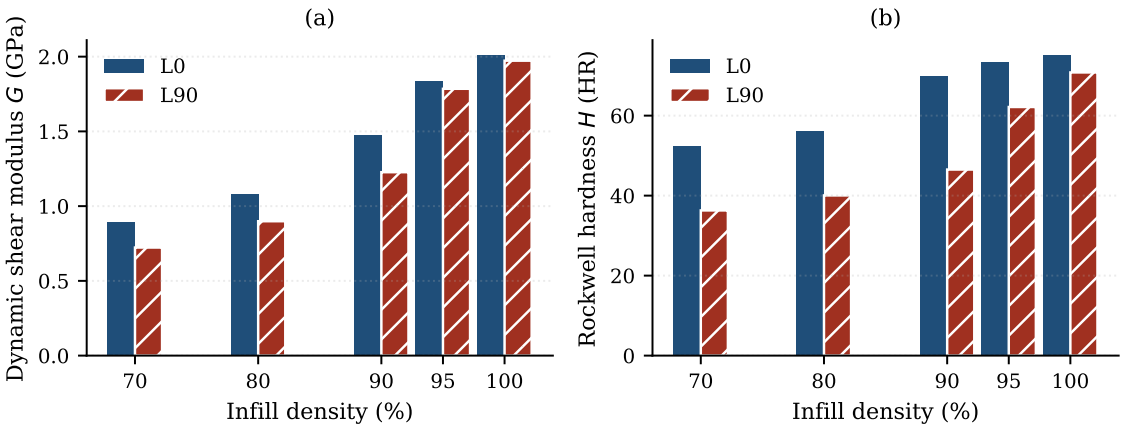


Figure 10. (a) Dynamic shear modulus and (b) Rockwell hardness as a function of infill density and raster orientation.

Hardness reveals the sharpest orientation effect in the whole data set. At 100 % infill the two orientations differ by only 5.8 % ($H_{L90}/H_{L0} = 0.942$), but at 90 % the ratio falls to 0.667: the L90 specimens have already lost 34.3 % of their hardness while the L0 specimens have lost only 7.1 %. Shear modulus behaves similarly but less dramatically, the ratio falling from 0.982 to 0.832 over the same interval.

The mechanism is geometric. Rockwell hardness is a surface property governed by the support available beneath the indenter. In the L0 orientation the infill lines run the full 125 mm length of the specimen and remain nearly continuous beneath the top skin down to 90 % infill, so the indenter meets what is effectively solid material. In the L90 orientation the lines run across the width, are short, and are bonded only to the perimeter walls; as line spacing opens the skin becomes a thin plate on widely spaced ribs and deflects under the indenter. Hardness is therefore a *local* property in L90 and a *global* one in L0, which is precisely why, as Section 3.5 shows, a global vibration descriptor calibrates hardness well in one orientation and poorly in the other.

3.5. *Inverse calibrations and predictive error*

For practical use the relationship must be inverted: a property is to be estimated from a measured descriptor. Table 5 reports the four inverse calibrations for which the design permits leave-one-out assessment, and Figure 11 displays them with their leave-one-out error bands.

Table 5. Inverse calibrations (property estimated from descriptor) with leave-one-out predictive error. ρ_S is the Spearman rank correlation. $\mathrm{RMSE}_{\mathrm{fit}}$ is the in-sample residual root mean square; $\mathrm{RMSE}_{\mathrm{LOO}}$ is obtained from (14).

Orient.	Calibration equation	R^2	p	ρ_S	$\mathrm{RMSE}_{\mathrm{fit}}$	$\mathrm{RMSE}_{\mathrm{LOO}}$	Ratio	$\max \lvert e_{\mathrm{LOO}} \rvert$
L0	$G = -0.0048 + 10.903\, Z_{\mathrm{MZN}}$	0.9110	0.0116	1.00	0.127	0.186	1.46	0.333
L90	$G = -0.2954 + 1.0513\,(Z_\infty \times 10^5)$	0.8266	0.0324	1.00	0.203	0.298	1.47	0.531
L0	$H = 32.17 + 247.0\, Z_{\mathrm{MZN}}$	0.9901	0.0004	1.00	0.924	1.33	1.44	2.11
L90	$H = 9.07 + 27.37\,(Z_\infty \times 10^5)$	0.7609	0.0537	1.00	6.46	9.71	1.50	16.87

G in GPa, H in HR; errors in the same units as the predicted property.

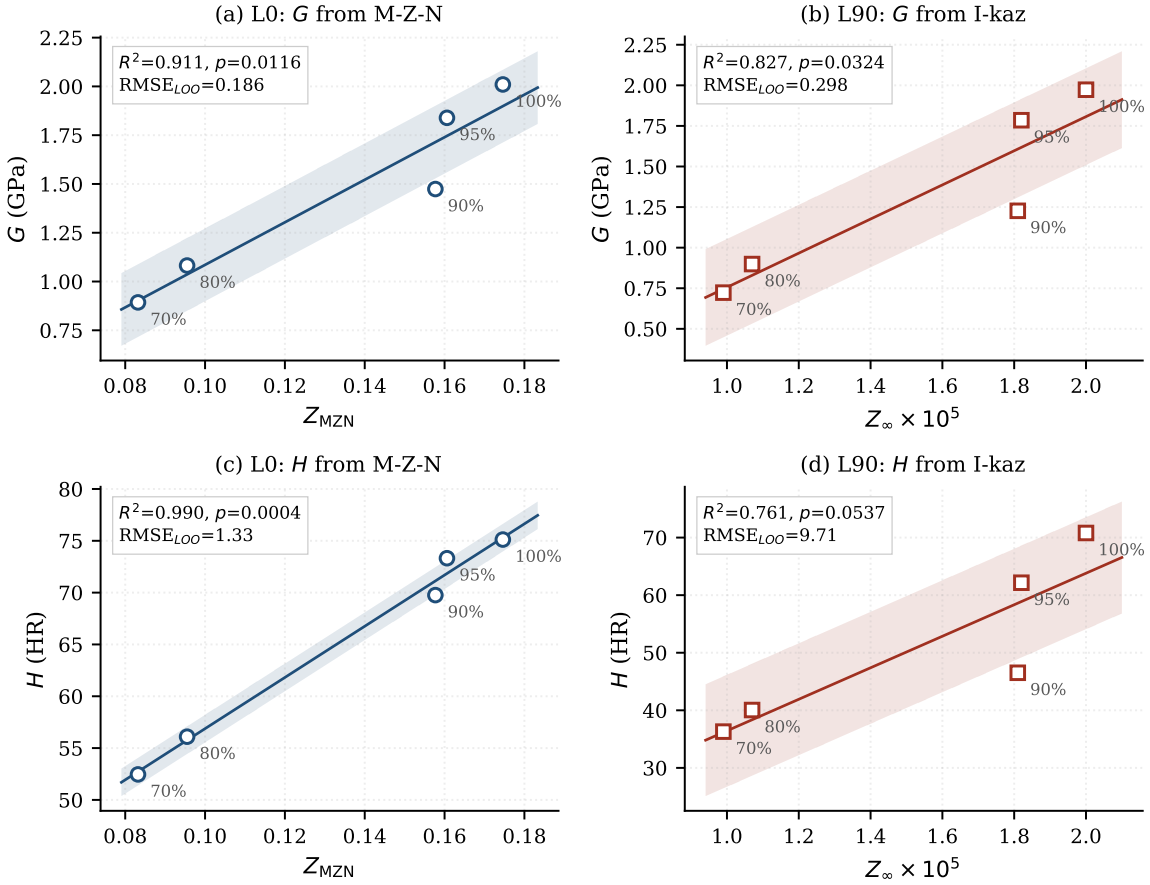


Figure 11. Inverse calibrations with leave-one-out error bands ($\pm\mathrm{RMSE}_{\mathrm{LOO}}$). Point labels give infill density. (a) and (c) L0 specimens calibrated by M-Z-N; (b) and (d) L90 specimens calibrated by I-kaz™.

Three results follow. First, the Spearman rank correlation is exactly 1.00 in all four cases: both descriptors order the five printing conditions perfectly by stiffness and by hardness, even where the linear fit is weak. Ranking is a more robust claim than numerical prediction, and it is the claim this design supports most securely.

Second, the leave-one-out error exceeds the in-sample residual by 44–50 % in every case. With five points, roughly one third of the apparent goodness of fit is attributable to the presence of the predicted point in the fitting set. This ratio is the most direct available statement of what $n = 5$ costs, and it is stable across all four calibrations, which suggests it is a property of the design rather than of any particular relationship.

Third, predictive utility differs sharply by orientation. In L0, M-Z-N estimates hardness to ± 1.3 HR (2.0 % of the mean) and shear modulus to ±0.19 GPa (13 %) under cross-validation. In L90, I-kaz^{TM} estimates hardness only to ± 9.7 HR (19 %), with a worst-case leave-one-out error of 16.9 HR at the 90 % design point. A L90 hardness calibration should therefore not be used for numerical estimation; classifying specimens into near-solid and porous groups is the defensible use.

3.6. Prediction intervals and residual diagnostics

A cross-validated point error states how far a prediction missed on average; it does not state how far the next prediction might miss. Table 6 therefore reports, for each inverse calibration, the 95 % prediction interval (15) together with the leverage, the largest internally studentised residual and the largest Cook's distance.

Table 6. Prediction intervals and influence diagnostics for the four inverse calibrations ($n = 5$, $\mathrm{df} = 3$). The interval half-width is evaluated at the mean descriptor value, which is its narrowest point; the range over the five design points is also given. $h_{\max}$ is the largest leverage, $|r|_{\max}$ the largest internally studentised residual and $D_{\max}$ the largest Cook's distance.

Orient.	Property	s	$\mathrm{RMSE}_{\mathrm{LOO}}$	95 % PI (at $\bar{x}$)	PI range	$h_{\max}$	$\lvert r\rvert_{\max}$	$D_{\max}$
L0	G (GPa)	0.164	0.186	± 0.57	± 0.59 to ± 0.66	0.57	1.72	0.57
L90	G (GPa)	0.262	0.298	± 0.91	± 0.94 to ± 1.03	0.54	1.72	0.58
L0	H (HR)	1.193	1.33	± 4.16	± 4.29 to ± 4.76	0.57	1.48	0.47
L90	H (HR)	8.340	9.71	± 29.1	± 30.1 to ± 32.9	0.54	1.71	0.58

s is the residual standard error. No Cook's distance exceeds the conventional $4/n = 0.80$ screening threshold, so no single point is formally influential by that criterion; leverage is nevertheless high at every point because $n = 5$.

Three things follow, and they qualify the earlier results rather than extend them.

First, the honest interval is about three times the leave-one-out error in every case. For shear modulus in the L0 orientation the leave-one-out error is 0.19 GPa but the 95 % prediction interval is ±0.57 GPa, which is 39 % of the mean shear modulus of that series. For hardness in L0 the corresponding figures are 1.3 HR and ± 4.2 HR. Reporting the cross-validated error alone would therefore understate the uncertainty on a single estimate by a factor of roughly three.

Second, one of the four relationships fails as a numerical estimator on its own terms. The L90 hardness calibration has a prediction interval of ± 29 HR against a series mean of 51.2 HR: an interval that spans more than the entire measured range of 36.3–70.8 HR. That calibration should not be used to estimate a hardness value, and we do not present it as one. Its only defensible use is the ordering it preserves, discussed below.

Third, the residual structure is the same in all four fits and is informative rather than alarming. The largest residual is at 90 % infill in three of the four calibrations and is negative in all three, with internally studentised residuals of -1.72, -1.72 and -1.71; this is the pattern examined in Section 3.7. No Cook's distance reaches the conventional $4/n$ screening threshold, so no point is formally influential. That result should be read cautiously: with five points the leverage is between 0.28 and 0.57 everywhere, every observation is structurally influential, and an influence statistic computed from three residual degrees of freedom has little power to detect an outlier. The diagnostics are therefore consistent with the fitted models but cannot be said to have tested them.

3.7. The 90 % infill anomaly

A pattern recurs across every relationship in this study and is visible in Figure 12: at 90 % infill the descriptors lag their mechanical counterparts. In the L0 orientation, shear modulus has fallen by 26.7 % relative to solid while M-Z-N has fallen by only 9.7 %; in L90, shear modulus has fallen by 37.8 % and hardness by 34.3 % while I-kaz^{TM} has fallen by 9.5 %. At 95 % infill the paired retention curves agree to within 3.2 percentage points in all three cases. At 80 and 70 % the agreement holds for L0 shear modulus (0.9 and 3.2 points) and L90 hardness (3.1 and 1.8 points) but not for L90 shear modulus, which has fallen 7.9 and 12.9 points further than the descriptor. What is common to all three pairings is that the 90 % point is the largest discrepancy by a wide margin — 17.0, 28.3 and 24.8 percentage points — and it is the largest residual in three of the four inverse calibrations of Table 5.

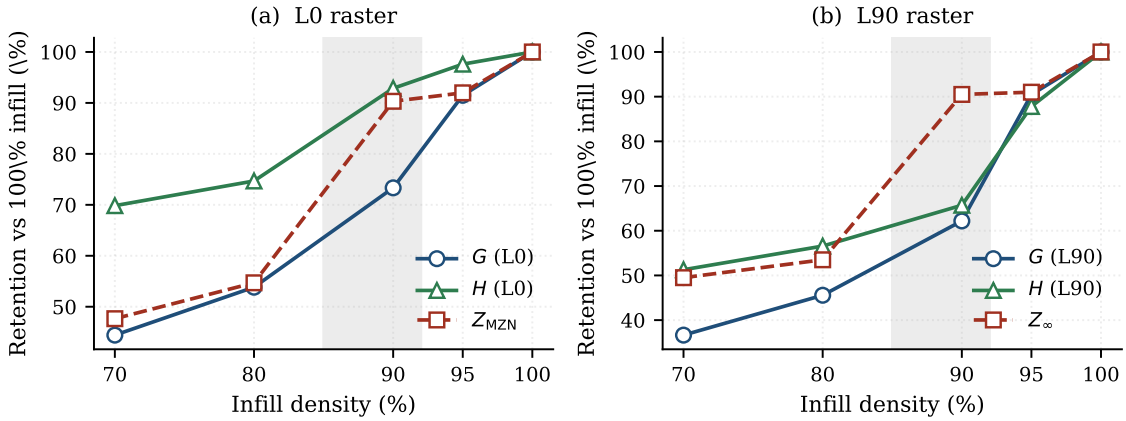


Figure 12. Retention of mechanical properties (solid lines) and of the statistical descriptors (dashed lines) relative to their 100 % infill values. The shaded band marks the 90 % design point, where the descriptors lag the mechanical properties in both orientations.

The interpretation offered below rests on a single design point and is therefore advanced as a hypothesis rather than a result. The most economical reading is that the descriptors are sensitive to the *onset of a cellular internal structure* rather than to gradual changes within a near-solid one. Between 100 and 90 % infill the deposited lines remain close enough to behave mechanically as a perforated solid; the ring-down amplitude and modulation that Z_∞ and Z_{MZN} measure change little. Below 90 % the spacing exceeds the extruded line width, the bar becomes a lattice, damping rises and the response shortens — and both descriptors drop sharply. Mechanical stiffness and hardness, by contrast, begin degrading as soon as any material is removed. The practical consequence is that these descriptors are well suited to detecting under-filled or cellular parts and poorly suited to resolving small density variations near full density. It also identifies the most informative place to add design points: the interval between 90 and 80 % infill, where the transition occurs. Until such points exist, the percolation-like reading of this behaviour remains conjectural: a single displaced observation in each of four correlated calibrations is equally consistent with an unmodelled feature of that one specimen. We have retained the physical account because it is testable and because it predicts where the additional points should be placed, not because the present data establish it.

3.8. Linear versus quadratic model selection

Table 7 compares the linear and quadratic specifications for all ten relationships; Figure 13 displays the comparison for the first six.

The comparison illustrates a point that is easy to obscure by reporting raw R^2 alone. The quadratic model has a higher or equal R^2 in all ten cases — as it must, since adding a regressor cannot increase the residual sum of squares — yet the *adjusted* R^2 falls in five of them, in one case dramatically (flexural stress vs I-kaz$^{\mathrm{TM}}$: 0.6545 to 0.5806). The partial F-test never approaches significance ($0.278 \le p \le 0.975$), and with $n = 5$ the quadratic model leaves only two residual degrees of freedom, so its apparent improvement carries almost no evidential weight.

Three relationships deserve comment because the quadratic term does raise the adjusted R^2: the two shear-modulus calibrations and the L90 hardness calibration. In each the improvement is driven entirely by the 90 % design point discussed in Section 3.7. A quadratic term can absorb a single displaced point, but doing so is curve-fitting rather than modelling: the physical account of that point is a threshold transition between a perforated solid and a lattice, which is a change of regime, not a smooth curvature. Fitting a parabola through the transition would extrapolate badly in both directions. Where a wider infill range is available, a segmented or two-regime model would be the principled alternative; within the present range the linear form is retained.

Combined with the absence of any physical mechanism that would produce smooth curvature within a 70–100 % infill window, this evidence supports retaining the linear specification for all ten relationships. The linear form also

Table 7. Linear versus quadratic model comparison. F is the partial F statistic (12) on the additional quadratic term, distributed as $F_{1,2}$ under H_0. The linear model is retained in every case.

Relationship	Orient.	n	Linear R^2	Linear R^2_{adj}	Quad. R^2	Quad. R^2_{adj}	F (p)	Selected (reason)
Flexural stress vs M-Z-N	L0	5	0.8725	0.8300	0.9371	0.8742	2.053 (0.288)	Linear (n.s.; parsimony)
Young's modulus vs M-Z-N	L0	5	0.9853	0.9804	0.9926	0.9853	2.004 (0.293)	Linear (n.s.; parsimony)
Density vs M-Z-N	L0	5	0.9549	0.9399	0.9550	0.9100	0.005 (0.951)	Linear ($R^2_{\text{adj}}\downarrow$)
Flexural stress vs I-kaz$^{\text{TM}}$	L90	5	0.7409	0.6545	0.7903	0.5806	0.472 (0.563)	Linear ($R^2_{\text{adj}}\downarrow$)
Young's modulus vs I-kaz$^{\text{TM}}$	L90	5	0.9126	0.8835	0.9171	0.8342	0.108 (0.773)	Linear ($R^2_{\text{adj}}\downarrow$)
Density vs I-kaz$^{\text{TM}}$	L90	5	0.9088	0.8784	0.9089	0.8177	0.001 (0.975)	Linear ($R^2_{\text{adj}}\downarrow$)
Hardness vs M-Z-N	L0	5	0.9901	0.9868	0.9909	0.9818	0.179 (0.713)	Linear (n.s.; parsimony)
Shear modulus vs M-Z-N	L0	5	0.9110	0.8814	0.9575	0.9149	2.181 (0.278)	Linear (n.s.; 90% regime)
Hardness vs I-kaz$^{\text{TM}}$	L90	5	0.7609	0.6812	0.8772	0.7545	1.896 (0.302)	Linear (n.s.; 90% regime)
Shear modulus vs I-kaz$^{\text{TM}}$	L90	5	0.8266	0.7688	0.9144	0.8288	2.050 (0.289)	Linear (n.s.; 90% regime)

n.s. = the additional quadratic term is not statistically significant. $R^2_{\text{adj}}\downarrow$ indicates that the adjusted coefficient of determination falls when the quadratic term is added. "90 % regime" indicates that the apparent quadratic improvement is driven entirely by the 90 % design point (Section 3.7).

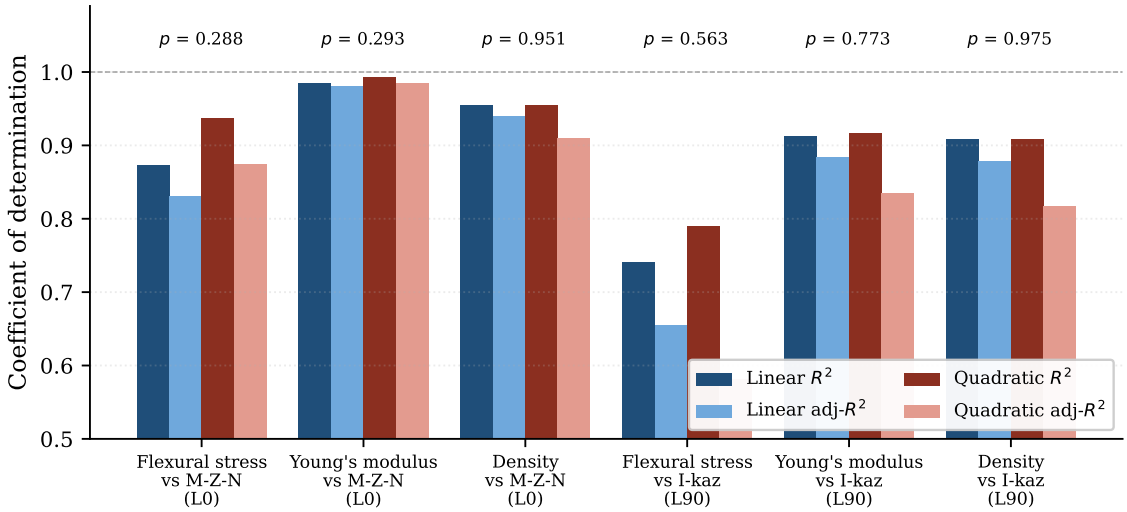


Figure 13. Linear versus quadratic model comparison across the six relationships. Raw R^2 never decreases when a term is added, but the adjusted R^2 falls in five of six cases, and the partial F-test on the quadratic term is non-significant throughout.

has the practical advantage of being directly invertible via (9), which a quadratic calibration is not without sign ambiguity.

3.9. Uncertainty of the calibration relationships

Table 8 reports interval estimates for the underlying correlation and for R^2, obtained through the Fisher transformation (13). These intervals are the most important statistical result in this paper, because they quantify how little a coefficient of determination computed from five points actually constrains.

Even the strongest relationship, Z_{MZN} against hardness, has a 95 % interval for R^2 of $[0.85,\ 0.999]$; for Z_{MZN} against Young's modulus the interval is $[0.79,\ 0.999]$, so the data are consistent with an underlying association explaining anywhere from about four fifths to essentially all of the variance. For density against I-kaz$^{\text{TM}}$ the interval runs from 0.20 to 0.994, and for both flexural stress and hardness against I-kaz$^{\text{TM}}$ the interval for r includes zero. A reader shown only the point estimates 0.9853 and 0.9088 would substantially overestimate the precision of

Table 8. Interval estimates for the population correlation and coefficient of determination, $n = 5$. Intervals were obtained via the Fisher z transformation; the standard error of z is $1/\sqrt{n-3} = 0.707$.

Relationship	Orient.	Point R^2	95% CI for r	95% CI for R^2
Flexural stress vs M-Z-N	L0	0.8725	[0.295, 0.996]	[0.087, 0.992]
Young's modulus vs M-Z-N	L0	0.9853	[0.888, 0.999]	[0.788, 0.999]
Density vs M-Z-N	L0	0.9549	[0.689, 0.999]	[0.474, 0.997]
Flexural stress vs I-kaz^{TM}	L90	0.7409	[−0.090, 0.991]	[0.000, 0.981]
Young's modulus vs I-kaz^{TM}	L90	0.9126	[0.465, 0.997]	[0.216, 0.994]
Density vs I-kaz^{TM}	L90	0.9088	[0.447, 0.997]	[0.200, 0.994]

these calibrations. Reporting the intervals does not weaken the finding that the descriptors track the mechanical properties — eight of ten slopes are significantly non-zero and all four inverse calibrations rank the conditions perfectly ($\rho_S = 1.00$) — but it does bound how confidently a numerical estimate of a property can be recovered from a measured coefficient. The leave-one-out errors in Table 5 give the same message in the units of the property itself, which is the more useful form for an engineer.

4. Discussion

4.1. Physical interpretation

The monotone increase of all three mechanical properties with infill density has a straightforward explanation: raising the infill fraction reduces internal void content, increases the load-bearing cross-section and improves continuity between deposited roads, so both stiffness and bending resistance increase. This agrees with the established FDM literature [11, 22, 32, 19]. The behaviour of the descriptors has the same origin viewed from the dynamic side. A specimen with fewer internal cavities attenuates the impulse less, sustains a more coherent decaying waveform and produces a signal whose amplitude distribution is both more energetic and more widely dispersed about its central value — exactly what Z_∞ and Z_{MZN} are constructed to measure [25, 26]. The step change in both descriptors between 80 and 90 % infill (Table 2) is consistent with a percolation-like transition from a discontinuous to a nearly continuous internal structure.

The anisotropy is equally interpretable. In the L90 configuration the deposited filaments run transverse to the specimen axis, so bending load is carried substantially along filaments rather than across inter-road interfaces; in L0 the load path crosses many weak interlayer bonds. The fact that density is orientation-independent while stiffness is not isolates the mechanism: the L90 advantage arises from filament alignment, not from a difference in material content. This reproduces the classical FDM anisotropy result [2, 16, 31] and supports the design recommendation that bending-loaded FDM components be printed in the L90 orientation to maximise the stiffness-to-weight ratio. The widening of the orientation gap as infill decreases indicates that anisotropy is itself a function of infill density, which is a practically relevant interaction: a part designed on the basis of 100 %-infill properties may be badly mis-specified if printed at 70 %.

4.2. What the coefficients of determination do and do not establish

The relationships reported in Table 3 are calibration fits, not validated predictive models, and the distinction matters. Four terms should be kept separate. *Correlation* describes the strength of linear co-variation and is what r measures. *Regression fit* describes how well a fitted line reproduces the data used to fit it, and is what R^2 measures. *Calibration* is the construction of a usable relationship between an instrument reading and a reference quantity, which is what equations (16)–(21) provide. *Validation* is the demonstration that the calibration performs acceptably on data not used to construct it — and no such demonstration is offered here, because no independent specimens were reserved.

The intervals in Table 8 make the cost of $n = 5$ explicit. With three residual degrees of freedom, a single influential design point can move R^2 substantially, and the Fisher intervals are correspondingly wide. It is worth

noting that the descriptor values in Table 2 are not evenly distributed: the 90 and 95 % points lie very close together (0.1577 and 0.1606 for M-Z-N; 18.10 and 18.20×10^{-6} for I-kaz$^{\mathrm{TM}}$), so the effective leverage of the design is concentrated in the extreme infill levels. This is a design feature worth changing in future work, since a more even spread of predictor values would tighten the slope estimates without requiring more specimens.

4.3. Direction of regression and inverse prediction

A further point deserves emphasis because it affects how these models can be used in practice. The models were fitted with the descriptor as response and the mechanical property as regressor, which is correct for a calibration experiment in which the property is the reference quantity. However, the intended *use* is the reverse: measure Z_∞ or Z_{MZN} non-destructively and infer E or ρ. That requires the inverse estimator (9), whose sampling distribution is not the forward one. The width of an inverse prediction interval depends on the slope magnitude, the residual variance and the distance of the new reading from the calibration mean, and it is strictly wider than the naive interval obtained by inverting the forward fit. Reporting R^2 from the forward regression therefore does not, on its own, characterise the accuracy with which a property could be recovered in service. Computing proper inverse prediction intervals requires the raw observation pairs and is listed in Section 5.

4.4. Independent calibration versus internal consistency

Section 2.6 separated the ten relationships into two classes, and the results justify keeping them separate. Eight relate a descriptor to a property measured by an entirely different instrument — a testing machine, a balance, a hardness tester. The two shear-modulus relationships do not: G is computed from the torsional resonance of the same transient that yields Z_∞ or Z_{MZN}. Their agreement ($R^2 = 0.911$ for L0, 0.827 for L90) shows that a time-domain scatter statistic and a frequency-domain peak extract consistent stiffness information from one signal. That is a worthwhile internal check — it would be troubling if they disagreed — but it is not evidence that vibration statistics predict mechanical behaviour, and it should not be pooled with the other eight when the strength of the method is assessed.

Reporting the two classes together without distinction would inflate the apparent evidence base by a quarter. The strongest genuinely independent result in this study is therefore the M-Z-N calibration of hardness in the L0 orientation ($R^2 = 0.9901$, $p = 0.0004$, $\mathrm{RMSE}_{\mathrm{LOO}} = 1.3$ HR), in which a scatter statistic computed from a 200 mm vibrating bar estimates an indentation measurement to within 2 %.

4.5. Why hardness calibrates well in one orientation and not the other

The hardness results in Sections 3.4 and 3.5 illustrate the boundary of the method more sharply than any other property. In L0 the descriptor predicts hardness almost exactly; in L90 it fails to reach the 5 % level ($p = 0.0537$) and its cross-validated error is 19 % of the mean. Both calibrations use the same experimental technique and the same infill range.

The explanation lies in the scale at which each property is determined. The descriptors summarise a *global* response: the whole bar rings, and Z_∞ and Z_{MZN} measure the amplitude and modulation of that ring-down. In L0, hardness is also effectively global — the continuous full-length infill lines beneath the surface mean that indentation resistance tracks the bulk solid fraction, and the two quantities move together. In L90, hardness becomes a local skin-on-ribs phenomenon: it begins to fall at 95 % infill, long before the global lattice opens, because the unsupported span between short transverse ribs starts to deflect. The global descriptor cannot see this, so the two diverge.

The general principle is that a global vibration descriptor calibrates a mechanical property to the extent that the property is itself governed by bulk structure. This gives a testable criterion for deciding in advance which properties are candidates for vibration-based estimation, and it predicts — consistently with our data — that bulk properties such as stiffness and density will calibrate more reliably than surface or local properties in orientations where those properties are locally controlled.

4.6. Method and orientation are confounded

The M-Z-N coefficient was computed only for L0 specimens and the I-kaz^{TM} coefficient only for L90 specimens. The two calibration sets therefore differ in *two* respects simultaneously: the statistical descriptor and the raster orientation. It follows that the numerical difference between, say, $R^2 = 0.9853$ for M-Z-N–modulus and $R^2 = 0.9126$ for I-kaz^{TM}–modulus cannot be attributed to the descriptors. Any statement of the form "M-Z-N is a better predictor than I-kaz^{TM}" would confound method with orientation and is not supported by this design. The two sets of results are presented here as *orientation-specific proof-of-concept calibrations*: each quantifies the performance of one descriptor under the single orientation on which it was evaluated.

This is not a minor caveat. The mechanical behaviour of the two orientations differs sharply — at 70 % infill the L0 modulus is about one fifth of the L90 value — so the two calibrations operate over very different property ranges, and the L0 set spans a far wider range of Young's modulus (0.471–3.263 GPa) than the L90 set (2.256–3.344 GPa). A wider predictor range mechanically inflates R^2 for a fixed residual variance, which is an additional reason the two R^2 values are not comparable. A crossed design, in which both descriptors are computed on both orientations, would permit an analysis of covariance on the regression coefficients and would separate descriptor effects from orientation effects. That experiment is the natural next step.

4.7. Relation to previous work

The results extend to additively manufactured polymers a line of work previously developed on metals. Nuawi et al. [26] showed that the M-Z-N coefficient of an impulse-excited acoustic signal tracks the elastic properties of cast iron, carbon steel, stainless steel and brass, and Nuawi et al. [27] extended the approach to fatigue strength. Bahari et al. [10] compared I-kaz^{TM} and M-Z-N for Young's modulus determination in metals, applying M-Z-N to the acoustic channel and I-kaz^{TM} to the piezoelectric channel — a signal-type split analogous to, and subject to the same interpretive constraint as, the orientation split in the present study. For polymers the available evidence is thinner: Ziyad et al. [33] characterised polymer specimens with I-kaz^{TM} under impact hammer excitation, and the present authors' earlier work [23] reported preliminary statistical signal analysis of polymer properties. The contribution here is to report the relationships with interval estimates, formal model selection and an explicit statement of the confound, rather than with point estimates alone.

It is worth stating precisely where this leaves the present study relative to the two closest precedents, since the descriptors themselves are not new. As noted above, neither [33] nor the authors' own earlier report [23] accompanies its descriptor–property relationships with interval estimates, model-selection evidence or cross-validated error. What is added here is therefore neither a descriptor nor a signal-processing step, but that inferential apparatus: interval estimates for the correlation, a formal linear-versus-quadratic comparison, leave-one-out cross-validation, classical-calibration prediction intervals, influence diagnostics, and an explicit statement of which relationships are independent evidence and which are internal consistency checks. The substantive new empirical content is the orientation contrast in the hardness relationships (Section 3.4) and the behaviour at 90 % infill (Section 3.7). We regard this as an incremental contribution, and the claims in Section 6 are scaled accordingly.

It is also relevant that [26] found *quadratic* relationships between the M-Z-N coefficient and impact force for metals. The linear specification adopted here is not in tension with that result: the predictor differs (a mechanical property across an infill series, rather than excitation force at fixed material), and within the narrow 70–100 % window no curvature is statistically detectable (Table 7). Should the infill range be extended downward, curvature may well emerge, and the linear form should not be extrapolated outside the calibrated interval.

4.8. Practical implications

Within the calibrated range, the results indicate that a single scalar computed from one impulse response tracks the stiffness and apparent density of an FDM PLA part well enough to rank printing conditions, and — for one of the four relationships examined — well enough to screen an individual part, at the resolution quantified below. The practical value is in process monitoring rather than in replacing standardised testing: a descriptor measured on every part, compared against a calibration established on a small destructively tested sample of the same geometry and orientation, would flag parts whose internal structure departs from the intended one. The measurement is fast,

requires no specimen preparation beyond mounting, and leaves the part intact. What the present evidence does not support is using equations (16)–(21) as general predictors of PLA properties across geometries, orientations, printers or infill ranges other than those calibrated here.

How such a screen would actually be operated It is worth being concrete, because the gap between a significant regression and a usable quality-control procedure is where methods of this kind normally fail. A manufacturer would destructively test a small set of parts of one geometry, printed in one orientation across the infill range of interest, and fit the calibration on that set. Every subsequent part would be impulse-excited on the same rig and its descriptor compared against that calibration. The decision the screen supports is a comparison, not a measurement.

What the screen can resolve. The detection limit is obtained by expressing the prediction intervals of Table 6 in infill units, using the slopes of the properties against infill density (0.841 HR and 0.0388 GPa per percentage point in L0; 1.138 HR and 0.0431 GPa in L90). The resulting figures are sobering and should be stated plainly. The best of the four routes is hardness in the L0 orientation, at $\pm 4.9\,\%$ infill; the L0 shear-modulus route gives $\pm 14.7\,\%$, and in L90 the two routes give $\pm 25.6\,\%$ and $\pm 21.1\,\%$ respectively. Only the first of these is a usable screen, and even it would flag a single part reliably only if its infill departed from target by about five percentage points. That is enough to catch an under-filled or mis-set build — the failure mode that matters most in practice, because it is usually gross — and nowhere near enough to certify a part to a stiffness tolerance. The three remaining routes resolve only large process departures. Averaging over several parts helps but does not rescue them: the interval on the mean of k parts has half-width $t\,s\sqrt{1/k + 1/n + (x_0 - \bar{x})^2/S_{xx}}$, which is bounded below by the calibration's own contribution and therefore cannot fall below 41 % of the single-part width however large k becomes. The floors are $\pm 2.0\,\%$ infill for hardness in L0, $\pm 6.0\,\%$ for shear modulus in L0, and $\pm 10.4\,\%$ and $\pm 8.6\,\%$ for the two L90 routes. Tightening the calibration itself — more design points and replication — is the only route to a finer screen.

What it costs. A three-point bend test consumes the specimen and occupies a universal testing machine; the impulse measurement takes a few seconds on a rig built from an accelerometer, a data acquisition module and a support frame, and the part survives. The economic case does not rest on the descriptor being as accurate as the destructive test — it plainly is not — but on the fact that it can be applied to every part rather than to a sampled few. Non-destructive screening is therefore preferable where the failure mode of interest is a gross process departure across a production run, and destructive testing remains necessary wherever an absolute property value must be certified.

What would have to be re-established on a new rig. Because the descriptors summarise the whole transient, they absorb the excitation energy, the sensor mass and mounting, and the support conditions. A calibration is therefore specific to a rig, a geometry and an orientation. Transfer to a different setup requires re-fitting the calibration on that setup; the functional form, and the ranking behaviour reported here, are what we would expect to carry over, not the coefficients. No transfer study was attempted in this work, and the conditions under which the coefficients might be portable remain an open question.

5. Limitations

The limitations below are stated in the order of their effect on the strength of the conclusions.

1. **Sample size.** Every calibration rests on $n = 5$ design points, one specimen per infill level, with three residual degrees of freedom. The resulting confidence intervals for R^2 (Table 8) are wide, and one influential point can materially change any fit. The consequence is quantitative and should not be softened: for the flexural stress calibration the 95 % interval for the population correlation runs from 0.295 to 0.996, so the data are consistent with anything from a weak association to a nearly deterministic one. A coefficient of determination of 0.87 computed from five points is not evidence of a strong relationship; it is evidence that a strong relationship has not been excluded. Every R^2 in this paper should be read alongside its interval in Table 8, and the model-selection results of Section 3.8 should likewise be regarded as exploratory, since a partial F-test on two residual degrees of freedom cannot discriminate sharply between specifications.

2. **No replication.** With a single specimen per configuration, measurement error cannot be separated from specimen-to-specimen variability, no standard deviations can be attached to the mechanical properties, and no pure-error estimate is available for a lack-of-fit test. This is the single most consequential deficiency in the design, and it is structural rather than presentational: every residual in Table 6 conflates the two sources of variation, so the residual standard error that drives every prediction interval cannot be decomposed. Three specimens per configuration would resolve it, and no amount of additional statistical treatment of the present data can substitute for them.

3. **Two specimen geometries.** Flexural properties were measured on ASTM D790 bars ($125 \times 12.7 \times 3.2\,\mathrm{mm}$) and the vibration descriptors on larger IET bars ($200 \times 50 \times 10\,\mathrm{mm}$). The calibrations therefore relate properties of a printing *condition*, not of an individual part, and their residual variance includes between-specimen variability.

4. **Two of the ten relationships are not independent.** The shear-modulus calibrations relate two functionals of the same recorded transient (Section 4.4) and are internal consistency checks rather than independent evidence.

5. **No independent validation.** No specimens were held out, and at $n = 5$ a train/test split is not defensible. No model in this paper is validated, and none is described as such.

6. **Method–orientation confounding.** M-Z-N was evaluated only on L0 specimens and I-kaz$^{\mathrm{TM}}$ only on L90 specimens (Section 4.6), so no comparison between the two descriptors is possible. The confound is complete, not partial: there is no cell of the design in which the two descriptors are observed under the same orientation, so no statistical adjustment can separate them. Any apparent difference in performance between M-Z-N and I-kaz$^{\mathrm{TM}}$ in this paper is uninterpretable, and we make no such comparison anywhere in the text.

7. **Unequal predictor ranges.** The L0 calibration spans a much wider modulus range than the L90 calibration, which affects R^2 independently of model quality.

8. **Narrow and uneven infill range.** Only 70–100 % infill was examined, and the 90 and 95 % design points are nearly coincident in descriptor value. Conclusions do not extend to sparse infills, and the design carries less information than five points could. The cost is not, however, the one that might be expected, and we computed it rather than asserting it. In descriptor space the five design points are in fact better spread than five evenly spaced values over the same range: the corrected sum of squares S_{xx} is 34 % larger in L0 and 39 % larger in L90 than an even spacing would give, and the maximum leverage is 0.57 and 0.54 respectively against the 0.60 that even spacing would produce (Table 6). The unevenness therefore does not widen the slope or prediction intervals. What it costs is resolution of the *shape* of the relationship: the 80–90 % interval, in which Section 3.7 localises a regime change, is spanned by a single gap, so no design point can distinguish a gradual transition from an abrupt one. The loss is of information about functional form, not of precision, and it is why additional levels in that interval appear as the third item in the programme below.

9. **Single material, printer and pattern.** One PLA grade, one desktop printer and a line infill pattern. Layer thickness, nozzle and bed temperature and print speed were held constant and their interactions with the descriptors are unexamined.

10. **Setup dependence.** The descriptors depend on impulse energy, sensor type and mounting, and boundary conditions. A calibration obtained on this rig is not transferable to another without re-calibration.

11. **Inverse prediction is bounded by wide intervals.** Cross-validated errors are reported for four calibrations (Table 5), but at $n = 5$ these are themselves high-variance. The classical-calibration prediction intervals of Table 6 are the honest bound on predictive use, and they are roughly three times the leave-one-out errors; for hardness in the L90 orientation the interval spans more than the entire measured range of the property, so that relationship carries no usable predictive information at all.

12. **Incomplete reporting of the acquisition chain and of indentation scatter.** The sample rate, record length, segmentation used in the descriptor averages and the impact-to-impact repeatability were not archived with

the results, and the individual Rockwell indentations behind each reported mean were not retained. Neither gap affects the regressions reported here, which are computed from the tabulated values, but both limit exact reproduction of the descriptor values by an independent group and prevent measurement uncertainty from being propagated into the calibration standard errors.

Priorities for further work

The limitations above define a concrete programme for extending this study. Each item below is stated with the experimental provision it requires.

1. **A crossed descriptor–orientation design.** Computing both I-kaz^{TM} and M-Z-N on both raster orientations would break the confound of Section 4.6 and allow an analysis of covariance to test whether the regression slopes differ by descriptor, by orientation, or both. This is the single change that would most increase the inferential value of the work, and it requires no new specimens — only that both descriptors be computed from the existing records.

2. **Replication at each configuration.** Three or more specimens per infill–orientation combination would separate measurement error from specimen-to-specimen variability, permit standard deviations and error bars on every reported property, and provide the pure-error estimate needed for a lack-of-fit test against the linear specification.

3. **Design points between 80 and 90 % infill.** Section 3.7 localises a regime change to this interval. Adding two or three levels there would resolve the transition, and test whether a segmented model outperforms the linear one. As Section 5 records, the present spacing does not cost slope precision; what the additional levels would buy is resolution of the functional form across the interval in which the regime change falls.

4. **Small-sample and resampling approaches as sensitivity checks.** Once replicated data exist, Bayesian calibration with weakly informative priors and bootstrap resampling of the inverse estimator should be run alongside the classical intervals reported here. Their value is as a check on whether the normal-theory intervals of Table 6 are optimistic, not as a means of extracting more from five points than five points contain.

5. **A transfer study.** Specimens printed on a different machine, from a different filament batch, and excited on an independently assembled rig would establish whether the functional form and the ranking behaviour survive a change of setup while the coefficients are re-fitted. This is the minimum evidence needed before the method could be described as portable.

6. **An independent validation set.** Specimens printed and tested after the calibration is fixed, and not used in fitting, would convert the present cross-validated error estimates into genuine validation. Until this is done, no model in this paper should be described as validated.

7. **Propagation of measurement uncertainty into the intervals.** The prediction intervals of Table 6 account for uncertainty in the calibration line and in the new reading, but their residual standard error still conflates measurement error with specimen-to-specimen variability. Replicate specimens, together with repeated indentations and repeated impacts recorded individually, would allow the two components to be separated and the intervals to be decomposed into a measurement part and a process part.

8. **Randomised print and test order.** The present design does not record randomisation of the order in which specimens were printed and tested, so slow drift in filament condition, nozzle state or ambient conditions cannot be excluded as a contribution to the apparent descriptor–property relationship. Randomising both orders, and recording them, should be standard practice in the replicated design.

9. **Extension beyond a single material and geometry.** Transferability across PLA grades, printers, specimen geometries and infill patterns is untested. Because the descriptors depend on impulse energy, sensor mounting and boundary conditions, a transfer study would establish whether calibration constants or only the functional form carry over.

10. **Local versus bulk properties.** The contrast between the L0 and L90 hardness calibrations (Section 4.5) suggests that a global descriptor calibrates a property in proportion to the extent that the property is bulk-controlled. This is a testable hypothesis: measuring a clearly local property and a clearly bulk property on the same specimens would confirm or refute it.

6. Conclusion

This study examined whether statistical descriptors of an impulse-excitation vibration signal can be related quantitatively to the mechanical properties of 3D-printed PLA, and with what statistical confidence. Ten specimen configurations — five infill densities from 70 to 100 % in two raster orientations — were characterised for flexural stress, Young's modulus, apparent density, dynamic shear modulus and Rockwell hardness, and their impulse responses were summarised by the I-kaz$^{\text{TM}}$ coefficient (L90 specimens) and the M-Z-N coefficient (L0 specimens).

Infill density governed every property, all of which changed monotonically over the range examined. Raster orientation produced strong anisotropy in stiffness, strength and hardness but essentially none in density, isolating filament alignment rather than material content as the source of the L90 advantage in bending. Both descriptors increased monotonically with infill, by 110 % (M-Z-N) and 102 % (I-kaz$^{\text{TM}}$).

Ten linear calibrations were fitted and compared against quadratic alternatives. The linear specification was retained throughout: the additional quadratic term was never significant ($0.278 \leq p \leq 0.975$), and where it raised the adjusted R^2 it did so only by absorbing a single design point. The strongest relationship was M-Z-N against hardness for L0 specimens ($R^2 = 0.9901$, $p = 0.0004$), followed by M-Z-N against Young's modulus ($R^2 = 0.9853$, $p = 0.0008$) and against density ($R^2 = 0.9549$, $p = 0.0041$). For L90 specimens, I-kaz$^{\text{TM}}$ gave $R^2 = 0.9126$ ($p = 0.0113$) with Young's modulus and $R^2 = 0.9088$ ($p = 0.0120$) with density. Two relationships did not reach the 5 % level: I-kaz$^{\text{TM}}$ against flexural stress ($p = 0.0611$) and against hardness ($p = 0.0537$).

What can legitimately be claimed is, first, that both descriptors rank the five printing conditions perfectly by stiffness and by hardness ($\rho_S = 1.00$ in every case), which is the most robust result in the study; and second, that within the calibrated range and for this specimen geometry, printer and test configuration, a single scalar derived from the impulse response tracks hardness and shear modulus closely enough to rank printing conditions, and — in the L0 orientation, for hardness — closely enough to screen an individual part against a target infill to within about five percentage points. The numerical bound on that use is the prediction interval rather than the cross-validated error: in the L0 orientation a hardness estimate carries ± 4.2 HR and a shear-modulus estimate ±0.57 GPa at 95 % confidence, roughly three times the corresponding leave-one-out figures of 1.3 HR and 0.19 GPa. What the design does not support is the word *validated*, or any numerical use of the L90 hardness relationship, whose prediction interval of ± 29 HR spans more than the entire measured range of the property itself. What cannot be claimed is comparable accuracy in L90, where the cross-validated hardness error reaches 19 % of the mean; nor predictive validity in general, since with $n = 5$ the leave-one-out error exceeds the in-sample residual by 44–50 % in every calibration and no independent validation was performed. Nor can either descriptor be said to outperform the other, since each was evaluated on only one raster orientation, confounding method with orientation.

Two findings have implications beyond this data set. The descriptors lag their mechanical counterparts at 90 % infill in every relationship. The reading we offer of that pattern — that the descriptors respond to the onset of a cellular internal structure rather than to gradual change within a near-solid one — is advanced as a hypothesis rather than a conclusion, because it rests on a single design point. The pattern itself bounds the resolution of the method near full density and identifies the 80–90 % interval as the most informative place to add design points. And the contrast between the L0 and L90 hardness calibrations suggests a general criterion: a global vibration descriptor calibrates a mechanical property to the extent that the property is itself governed by bulk rather than local structure.

The priorities for subsequent work follow directly from the limitations: compute both descriptors on both orientations in a crossed design so that method and orientation can be separated; replicate each configuration so that measurement and specimen variability can be distinguished and lack of fit tested; add design points between 80 and 90 % infill to resolve the transition; and reserve an independent specimen set so that the calibrations can be validated rather than merely fitted and cross-validated.

Acknowledgement

The authors thank the Electromechanical Systems Laboratory (LASEM), University of Sfax, for additive manufacturing and laboratory facilities, and the Department of Mechanical Engineering, Universiti Kebangsaan Malaysia, for access to the NI 9234 data acquisition system. The support of the Department of Mechanical Power Techniques Engineering, University of Al Maarif, is gratefully acknowledged.

The authors declare no competing financial interests or personal relationships that could have appeared to influence the work reported in this paper. No specific grant was received from any funding agency in the public, commercial or not-for-profit sectors. The data supporting the findings of this study are available from the corresponding author on reasonable request.

REFERENCES

1. R. D. Adams, and P. Cawley, *A review of defect types and nondestructive testing techniques for composites and bonded joints*, NDT International, vol. 21, no. 4, pp. 208–222, 1988.
2. S. H. Ahn, M. Montero, D. Odell, S. Roundy, and P. K. Wright, *Anisotropic material properties of fused deposition modeling ABS*, Rapid Prototyping Journal, vol. 8, no. 4, pp. 248–257, 2002.
3. M. Alfano, and L. Pagnotta, *A non-destructive technique for the elastic characterization of thin isotropic plates*, NDT & E International, vol. 40, no. 2, pp. 112–120, 2007.
4. ASTM International, *ASTM D638: Standard Test Method for Tensile Properties of Plastics*, ASTM International, West Conshohocken, PA.
5. ASTM International, *ASTM D790-17: Standard Test Methods for Flexural Properties of Unreinforced and Reinforced Plastics and Electrical Insulating Materials*, ASTM International, West Conshohocken, PA, 2017.
6. ASTM International, *ASTM D785: Standard Test Method for Rockwell Hardness of Plastics and Electrical Insulating Materials*, ASTM International, West Conshohocken, PA.
7. ASTM International, *ASTM E1876-15: Standard Test Method for Dynamic Young's Modulus, Shear Modulus, and Poisson's Ratio by Impulse Excitation of Vibration*, ASTM International, West Conshohocken, PA, 2015.
8. G. Atakok, M. Kam, and H. B. Koc, *Tensile, three-point bending and impact strength of 3D printed parts using PLA and recycled PLA filaments: a statistical investigation*, Journal of Materials Research and Technology, vol. 18, pp. 1542–1554, 2022. doi:10.1016/j.jmrt.2022.03.013
9. R. Auras, B. Harte, and S. Selke, *An overview of polylactides as packaging materials*, Macromolecular Bioscience, vol. 4, no. 9, pp. 835–864, 2004.
10. A. R. Bahari, M. Z. Nuawi, S. Abdullah, A. K. Ariffin, and Z. M. Nopiah, *Comparison of Young's modulus property determination of metallic materials under two statistical analysis methods*, Jurnal Teknologi (Sciences & Engineering), vol. 78, no. 6–10, pp. 23–29, 2016.
11. J. M. Chacón, M. A. Caminero, E. García-Plaza, and P. J. Núñez, *Additive manufacturing of PLA structures using fused deposition modelling: effect of process parameters on mechanical properties and their optimal selection*, Materials & Design, vol. 124, pp. 143–157, 2017.
12. E. Cuan-Urquizo, E. Barocio, V. Tejada-Ortigoza, R. B. Pipes, C. A. Rodriguez, and A. Roman-Flores, *Characterization of the mechanical properties of FFF structures and materials: a review on the experimental, computational and theoretical approaches*, Materials, vol. 12, no. 6, article 895, 2019.
13. S. Dhouib, *Fast method for the mobile robot path planning problem: The DM-SPP method*, Statistics, Optimization and Information Computing, vol. 15, no. 1, pp. 516–528, 2026. doi:10.19139/soic-2310-5070-3013
14. S. Dhouib, M. Kammoun, S. Dhouib, and T. Loukil, *Supply chain networks optimization under uncertain environment with Dhouib-Matrix-TP1 heuristic*, Statistics, Optimization and Information Computing, vol. 13, no. 4, pp. 1505–1521, 2025. doi:10.19139/soic-2310-5070-2282
15. H. Doğanay Kati, F. He, M. Khan, H. Gökdağ, and Y. L. A. Alshammari, *Effect of printing parameters on the dynamic characteristics of additively manufactured ABS beams: An experimental modal analysis and response surface methodology*, Polymers, vol. 17, no. 12, article 1615, 2025. doi:10.3390/polym17121615
16. M. Domingo-Espin, J. M. Puigoriol-Forcada, A. A. Garcia-Granada, J. Llumà, S. Borros, and G. Reyes, *Mechanical property characterization and simulation of fused deposition modeling polycarbonate parts*, Materials & Design, vol. 83, pp. 670–677, 2015.
17. D. J. Ewins, *Modal Testing: Theory, Practice and Application*, 2nd ed., Research Studies Press, Baldock, 2000.
18. S. Farah, D. G. Anderson, and R. Langer, *Physical and mechanical properties of PLA, and their functions in widespread applications — a comprehensive review*, Advanced Drug Delivery Reviews, vol. 107, pp. 367–392, 2016.
19. E. Ftoutou, L. Allegue, H. Marouani, T. Hassine, Y. Fouad, and H. Mrad, *Modeling of effect of infill density percentage on rotating bending fatigue behavior of additive-manufactured PLA polymers*, Materials, vol. 17, no. 2, article 471, 2024. doi:10.3390/ma17020471
20. M. F. Ghazali, N. I. I. Mansor, M. Z. Nuawi, and J. A. Ghani, *Facile wear failure monitoring of commercial bearing alloys using I-kaz method*, Engineering Failure Analysis, vol. 35, pp. 545–553, 2013.
21. D. Kallel, N. Beji, and S. Dhouib, *Fuzzy analytical hierarchy process to optimize supply chain processes in the digital age*, Statistics, Optimization and Information Computing, vol. 15, no. 3, pp. 2267–2285, 2026. doi:10.19139/soic-2310-5070-3203

22. A. Lanzotti, M. Grasso, G. Staiano, and M. Martorelli, *The impact of process parameters on mechanical properties of parts fabricated in PLA with an open-source 3D printer*, Rapid Prototyping Journal, vol. 21, no. 5, pp. 604–617, 2015.
23. N. F. Mohammed, M. Z. Nuawi, and A. Elloumi, *Development of polymer properties characterisation using statistical signal analysis*, in Advances in Mechanical Engineering, Materials and Mechanics II (ICAMEM 2024), Lecture Notes in Mechanical Engineering, Springer, Cham, 2025. doi:10.1007/978-3-031-89733-7_35
24. T. D. Ngo, A. Kashani, G. Imbalzano, K. T. Q. Nguyen, and D. Hui, *Additive manufacturing (3D printing): a review of materials, methods, applications and challenges*, Composites Part B: Engineering, vol. 143, pp. 172–196, 2018.
25. M. Z. Nuawi, M. J. M. Nor, N. Jamaludin, S. Abdullah, F. Lamin, and C. K. E. Nizwan, *Development of integrated kurtosis-based algorithm for Z-filter technique*, Journal of Applied Sciences, vol. 8, no. 8, pp. 1541–1547, 2008.
26. M. Z. Nuawi, A. R. Bahari, S. Abdullah, A. K. A. M. Ihsan, and M. B. Ali, *Mesokurtosis zonal nonparametric signal analysis for dynamic characterisation of metallic material*, Jurnal Kejuruteraan, vol. 24, pp. 21–27, 2012.
27. M. Z. Nuawi, A. R. Bahari, S. Abdullah, A. K. Ariffin, and Z. M. Nopiah, *Time domain analysis method of the impulse vibro-acoustic signal for fatigue strength characterisation of metallic material*, Procedia Engineering, vol. 66, pp. 539–548, 2013.
28. L. Pagnotta, and G. Stigliano, *Assessment of elastic properties of isotropic plates by dynamic tests*, Experimental Mechanics, vol. 48, no. 1, pp. 37–45, 2008.
29. M. Pozhanka, A. Zagrai, F. Baez Avila, and B. Drach, *Application of ultrasonic testing for assessing the elastic properties of PLA manufactured by fused deposition modeling*, Applied Sciences, vol. 14, no. 17, article 7639, 2024. doi:10.3390/app14177639
30. D. Popescu, A. Zapciu, C. Amza, F. Baciu, and R. Marinescu, *FDM process parameters influence over the mechanical properties of polymer specimens: a review*, Polymer Testing, vol. 69, pp. 157–166, 2018.
31. B. Rankouhi, S. Javadpour, F. Delfanian, and T. Letcher, *Failure analysis and mechanical characterization of 3D printed ABS with respect to layer thickness and orientation*, Journal of Failure Analysis and Prevention, vol. 16, pp. 467–481, 2016.
32. J. A. Travieso-Rodriguez, R. Jerez-Mesa, J. Llumà, O. Traver-Ramos, G. Gomez-Gras, and J. J. Roa Rovira, *Mechanical properties of 3D-printing polylactic acid parts subjected to bending stress and fatigue testing*, Materials, vol. 12, no. 23, article 3859, 2019.
33. S. S. Ziyad, M. Z. Nuawi, T. T. Mohamed, A. R. Bahari, and F. M. Nadia, *Characterisation of polymer material using I-kaz™, analysis method under impact hammer excitation technique*, Journal of Applied Sciences, vol. 15, no. 1, pp. 138–145, 2015.